

AMERICAN UNIVERSITY OF BEIRUT

AN ELECTROMAGNETIC BIOMEDICAL 2.4 GHZ,
WEARABLE, NON-INVASIVE TRANSCEIVER FOR
CONTINUOUS BLOOD PRESSURE MONITORING

by
MONA KHALIL EL ABBASI

A dissertation
submitted in partial fulfillment of the requirements
for the degree of Doctor of Philosophy
to the Department of Electrical and Computer Engineering
at Maroun Semaan Faculty of Engineering and Architecture
at the American University of Beirut

Beirut, Lebanon
June 2022

AMERICAN UNIVERSITY OF BEIRUT

AN ELECTROMAGNETIC BIOMEDICAL 2.4 GHZ, WEARABLE, NON-INVASIVE TRANSCEIVER FOR CONTINUOUS BLOOD PRESSURE MONITORING

by
MONA KHALIL EL ABBASI

Approved by:



Dr. Karim Kabalan, Professor
Department of Electrical and Computer Engineering

Advisor


[Mervat Madi \(Jun 13, 2022 00:12 GMT+4\)](#)

Dr. Mervat Madi, Assistant Professor
Department of Electrical and Computer School, Amity University of Dubai

Co-Advisor



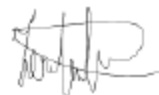
Dr. Ali Chehab, Professor
Department of Electrical and Computer Engineering

Chair of Committee



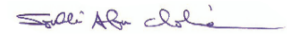
Dr. Nassir Hussni Sabah, Professor
Department of Electrical and Computer Engineering

Member of Committee



Dr. Hassan Artail, Professor
Department of Electrical and Computer Engineering

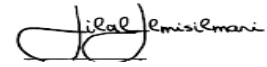
Member of Committee



Dr. Sobhi Abou Chahine, Professor

Member of Committee

Department of Electrical and Computer Engineering, Beirut Arab University



Dr. Hilal El Misilmani, Associate Professor

Member of Committee

Department of Electrical and Computer Engineering, Beirut Arab University

Date of dissertation defense: June 6, 2022

AMERICAN UNIVERSITY OF BEIRUT

THESIS RELEASE FORM

Student Name: El Abbasi Mona Khalil
Last First Middle

I authorize the American University of Beirut, to: (a) reproduce hard or electronic copies of my thesis; (b) include such copies in the archives and digital repositories of the University; and (c) make freely available such copies to third parties for research or educational purposes:

- ☐ As of the date of submission
- ☐ One year from the date of submission of my thesis.
- ☐ Two years from the date of submission of my thesis.
- ☒ Three years from the date of submission of my thesis.

Mona El Abbasi June 6, 2022

Signature

Date

ACKNOWLEDGEMENTS

First and foremost, I am extremely grateful to my supervisors, Prof. Karim Kabalan and Dr. Mervat Madi for their invaluable advice, continuous support, and patience during my PhD study. Their immense knowledge and plentiful experience have encouraged me in all the time of my academic research and daily life. I would like to thank all the committee members. It is their kind help and support. Lastly, I would like to express my gratitude to my parents. Without their tremendous understanding and encouragement in the past few years, it would be impossible for me to complete my study. I also appreciate all the support I received from the rest of my family.

ABSTRACT OF THE DISSERTATION OF

Mona Khalil ElAbbasi for Doctor of Philosophy
Major: Communications, RF and Electromagnetics

Title: An Electromagnetic Biomedical 2.4 Ghz, Wearable, Non-Invasive Transceiver for Continuous Blood Pressure Monitoring.

Abstract: Painless, cuffless and continuous blood pressure monitoring sensors provide a more dynamic measure of blood pressure for critical diagnosis or continuous monitoring of hypertensive patients compared to current cuff-based options. To this end, a novel flexible and wearable microstrip patch antenna topology is proposed to measure dynamic blood pressure (BP). The methodology was implemented on a simulated five-layer human tissue arm model created and designed in High-Frequency Simulation Software “HFSS”. The electrical properties of the five-layer human tissue were set at the frequency range (2–3) GHz to comply with clinical/engineering standards. The fabricated patch incorporated on a 0.4 mm epoxy substrate achieved consistency between the simulated and measured reflection coefficient results at flat and bent conditions over the frequency range of 2.3–2.6 GHz. Simulations for a 10 g average specific absorption rate (SAR) based on IEEE-Standard for a human arm at different input powers were also carried out. The safest input power was 50 mW with an acceptable SAR value of $3.89 \text{ W/Kg} < 4 \text{ W/Kg}$. This study also explored a novel method to obtain the pulse transit time (PTT) as an option to measure BP. Pulse transmit time is based on obtaining the time difference between the transmission coefficient scattering waveforms measured between the two pairs of metallic sensors underlying the assumption that brachial arterial geometries are dynamic. Consequently, the proposed model is validated by comparing it to the standard nonlinear Moens and Korteweg model over different artery thickness-radius ratios, showing excellent correlation between 0.76 ± 0.03 and 0.81 ± 0.03 with the systolic and diastolic BP results. The absolute risk of arterial blood pressure increased with the increase in brachial artery thickness-radius ratio. The results of both methods successfully demonstrate how the radius estimates, PTT and pulse wave velocity (PWV), along with electromagnetic (EM) antenna transmission propagation characteristics, can be used to estimate continuous BP non-invasively.

Keywords: microstrip patch antenna; transmission coefficient scattering parameter; specific absorption rate; Moens-Korteweg equation; brachial artery radius-to-tissue thickness ratio; blood pressure

TABLE OF CONTENTS

ACKNOWLEDGEMENTS	1
ABSTRACT	2
ILLUSTRATIONS	6
TABLES	9
INTRODUCTION	10
1.1 Thesis Objectives and Contributions	11
1.2 Thesis Organization	12
LITERATURE REVIEW	14
2.1 Introduction.....	14
2.2 What is Hypertension?.....	14
2.3 Location of Measurement	15
2.4 Previous Blood Pressure Measurement Methods	16
2.4.1 The Auscultatory Method	16
2.4.2 The Oscillometric Technique.....	18
2.4.3 Conclusion	18
2.5 Advances in Wearable Blood Pressure Estimation Technologies	20
2.6 Effect of Exposure of Electromagnetic Radiations on Human Body	28
FLEXIBLE WEARABLE MICROSTRIP ANTENNA FOR SKIN CONTACT APPLICATION	31

3.1 Theoretical Equations	31
3.2 Methodology	33
3.2.1 Flexible Antenna Geometry	33
3.2.2 Antenna Simulation in Bending Condition.....	38
3.2.3 Transmit/Receive Antennas in Free Space	40
DESIGN OF HUMAN ARM	42
4.1 Human-Tissue-Arm Equivalent Simulated Phantom Modeling	42
4.2 Specific Absorption Rate (SAR) Analysis vs. Power of an Average Simulated Human Arm Phantom	45
4.3 Testing an Antenna on Simulated and Real Human Arm.....	48
4.4 Transmit/Receive Antennas on a Simulated Heterogenous Human Arm phantom and a Real Human Arm	50
ARTERIAL BLOOD PRESSURE ESTIMATION USING TRANSMISSION COEFFICIENT AND DATA ANALYSIS BY MEANS OF ASSESSMENT OF BRACHIAL DIAMETER CHANGE.....	53
5.1 The Proposed Blood Pressure Determination Method	53
5.2 Why is Thickening of Artery Wall Important?.....	55
5.3 Method I: Direct Pulse Transit Time Method by Means of Assessment of Brachial Artery Diameter Change and Pulse Wave Velocity.	56
5.3.1 Measuring Transmission Coefficient (S₂₁) in Three Different Cases:.....	58
5.3.2 Computing PWV with PTT	59
5.3.3 Regression Equations to Find BP	61
5.2.4 Summary	63
5.4 Method II: Mathematical Approach Towards Pulse Wave Velocity Determination	63
5.4.1 Correlation Between Stiffness and PWV	64

5.5 Summary	72
CONCLUSION	73
6.1 Advantages.....	76
6.2 Limitations and Future Work.....	76
REFERENCES	78

ILLUSTRATIONS

Figure

2.1: Three basic types of blood pressure measurement devices [10].....	17
2.2: Indirect blood Sphygmomanometer measurement [10].	18
2.3: Illustrates the pulse wave velocity in brachial artery [15].	20
2.4: The ECG signal and PPG signal. PTT is the difference between the first peak of ECG and first peak of PPG [17].	21
2.5: Schematic of the overall system [23].....	24
2.6: Architecture of proposed NPNS based radar system for artery pulse signal detection [27].	26
2.7: Methodology of pulse wave velocity (PWV)-based blood pressure (BP) estimation [28].	27
2.8: System Design [28].....	27
3.1: (a) Conventional microstrip patch antenna versus (b) the proposed patch antenna.	34
3.2: The simulated parametric analysis on the length and width of slot of the proposed antenna.	35
3.3: (a) Optimizing antenna performance based on three truncating angles along with a slot inside the patch. (b) shows the geometry of the truncated-corner patch.	35
3.4: Designed flat patch antenna on epoxy flexible material: (a) front view and (b) bottom view.	37
3.5: Structure and performance measurement of the fabricated patch antenna: (a) schematic of fabricated antenna with coaxial feed on a flexible substrate; (b) photos of different antenna bending around cylinder of diameter 45mm and 60 mm; (c) variation of measured (dotted lines) and simulated (solid lines) reflection coefficient for different bending diameters; (d) simulated and measured off-body 2-D radiation patterns at 2.4 GHz of the proposed antenna in flat and at different bending conditions.	39
3.6: Cartesian plot of the radiation patterns between flat and bending diameters.	39
3.7: Two fabricated antennas in free space separated by 6.25 cm.	40
3.8: Simulated versus measured transmission coefficient between two antennas in free space.....	41
4.1: Relative permittivity (ϵ_r) in the frequency range from (2-3) GHz of the biological tissues selected for the heterogeneous simulated samples.	42
4.2: Cylindrical modeled multi-layer human arm model developed in ANSYS HFSS,	

(a) perspective view, (b) cross section of the top view (zoomed in).	44
4.3: The peak 10g SAR value at the surface of the arm.	46
4.4: Simulated total electric field strength at the absorbing conditions.....	46
4.5: The microstrip patch antenna on the simulated human arm model of (a) 45 mm radius versus (b) the fabricated microstrip patch antenna on real human arm subject of the same radius.	48
4.6: Simulated return loss with the presence of the simulated human arm model versus measured return loss on a real human arm of the same radius 45 mm as simulated.	49
4.7: The fabricated pair of antennas are placed on a real human arm of radius 45 mm to examine the transmission coefficient.....	51
4.8: show the measured versus the simulated transmission coefficient S_{21} response of a pairs of antennas in free space and on simulated human arm modeled close to the real human arm subject of radius 45mm respectively.	51
5.1. Illustration of proposed method related to brachial artery h/R ratio variation in respect to blood pressure estimation. Healthy elastic arteries=Normal BP and elastic artery stiffening= increase CV risk. The arterial vessel is often modeled as an elastic cylindrical tube. The simulation would be performed at five instances of brachial artery diameters to mimic the condition of blood flow. Although the above simulation model lacks blood flow, the consideration of different arterial diameters partly compensates for the hemodynamic effects The choice of different arterial diameters complies with the characteristics of the arterial system. It was reasonably assuming that the brachial artery diameter changes uniformly at each dielectric characteristic change of the flow of blood, fat, muscle, bone and skin	54
5.2: Brachial artery various thickness/radius ratio associated to blood pressure variations.....	55
5.3: Placement of patch antennas over brachial artery to detect blood pulse waveforms.....	57
5.4: A pair of transmitting/receiving antennas bent over cylindrical multi-layer human arm model developed in ANSYS HFSS. EM waves out of the antennas can reach the targeted brachial artery along with the wide dielectric characterization range. L = length from the first sensor to the second; PTT = time taken for the pulse wave to propagate from the upper side (1) to lower side of the brachial artery (2). Based on the methodology of this study, the PWV-PPT relationship was noted for three distinct cases reflecting the effect of blood flow and thus blood pressure estimation. The cases were investigated with different artery h/R ratios of 0.5, 0.7 and 0.9.	58
5.5: Three Cases of simulation results of transmission coefficient variation in the time domain for the human brachial artery of h/R ratios =0.5, 0.7 and 0.9 in time domain analysis. PTT is inversely related to BP through PWV calculation of first sensor and second sensor.	60

5.6: Simulation results of PTT- based pulse measurement dual sensors: Through this variation, PTT estimates for human artery of thickness/radius ratio $h/R=0.5, 0.7$ and 0.9 . PTT are extracted and then PWV can be calculated to provide a comprehensive overview of the blood pressure variation level.	61
5.7: Mean BP versus PWV for the brachial artery of h/R ratios of $0.5, 0.7$ and 0.9 , with linear regression trend line. In addition, the relationship of PTT to Systolic BP with a straight line representing linear regression and the relationship of PTT to Diastolic BP with a straight line representing linear regression.	62
5.8: The theoretical, i.e., Moens-Korteweg, relationship between the PWV versus artery stiffness (equivalent modulus) E (based on the parameters used in the simulation) for a human brachial artery before deformation due to the blood pressure.	66
5.9: The theoretical, i.e., Moens-Korteweg, relationship between the PWV versus artery stiffness (equivalent modulus) E for a human brachial artery after deformation due to blood pressure.	68
5.10: Blood pressure P versus normalized PWV for human brachial artery. Effects of wall thickness divided by vessel radius in arterioles (after deformation) on blood pressure (in mmHg). At any level of mean arterial pressure, the absolute risk of a composite cardiovascular outcome increased in relation to aortic PWV.	69
5.11: Relationship between pulse-wave velocity and systolic blood pressure (in mmHg).	70
5.12: Relationship between pulse-wave velocity and diastolic blood pressure (in mmHg).	71

TABLES

Table

2.1: Healthy and unhealthy blood pressure ranges [2].....	15
2.2: Comparison of the methods of blood pressure measurement [9].	19
2.3: Main error factor of the methods of blood pressure measurement [9,11]. ..	20
3.1. Optimized dimensions of the simulated patch antenna parameters.....	36
3.2. Change in radiation characteristics of antenna with bending.	40
4.1: Dispersion characteristics of human tissue layers at 2.4 GHz.....	43
4.2: Simulated SAR in ten grams of arm tissue obtained from HFSS for the antennas placed at both sides of the human arm.....	47
5.1: Summary of estimated PTT, PWV and mean BP in the three studied cases.	63
5.2: Summary of PWV and E estimates for different values of h/R ratios before artery deformation.....	65
5.3: Summary of PWV and E estimates for different values of Thickness/Radius ratio (h/R) after deformation due to blood pressure.	67
5.4: Summary table comparing the two proposed methods for blood pressure estimation.....	72

CHAPTER 1

INTRODUCTION

Globally, the incidence of cardiovascular disease (CVD) is one of the leading causes of world-wide morbidity and mortality. Blood pressure (BP) elevation is also a common risk factor for cardiovascular disorders, including stroke and heart failure [1]. It is currently one of the top ten causes of death worldwide. Chronic disease conditions are often related to elevated BP levels [1]. Blood pressure is primarily measured to control patients with serious health conditions such as hypertension or after a heart attack [2].

Although blood pressure is routinely measured during a healthcare visit, the traditional oscillometric method with a sphygmomanometer may cause discomfort to users and does not provide data about continuous variations in BP during either daily activities or at rest. Noninvasive intermittent techniques [3] are the most common methods currently in use, such as by auscultatory at-home devices. At-home devices are simpler, quicker, and require less expertise to use, but they are also often less accurate. They also provide, in most cases, only a one-time measure of BP, while arterial blood pressure fluctuates continuously. The available non-invasive continuous BP monitoring devices include the arterial tonometry method, vascular unloading technique, and pulse waveform characteristic parameter method, which are all sensitive to movement, more expensive, and need to be checked frequently for accuracy [4-6]. They also provide, in most cases, only one "snap-shot" measure at a time, while true arterial blood pressure fluctuates continuously. However, they are all sensitive to movement, more expensive and need to be checked frequently for accuracy.

Recently, researchers have been focusing on electromagnetic (EM) wave sensing

and microstrip patch antennas as a leading technology due to the EM interactions of scattering, reflection, absorption and transmission inside the human body that allows specific physiological features such as blood pressure to be determined. The microstrip patch antennas are metallic sensors that can radiate and receive EM waves [7]. The properties of the reflected and transmitted EM waves, in terms of scattering parameters (S parameters), are used to determine and analyze the BP levels. S parameters (S_{11} , S_{12} , S_{21} and S_{22}) are defined as the input-output relationship between terminals of the EM sensors [7].

1.1 Thesis Objectives and Contributions

This thesis work has the goal of estimating BP through the study of a small-sized and low-power noninvasive measurement sensors for measuring blood pressure pulsations in the brachial artery. These pulsations can be used to determine blood pressure, which is undoubtedly the most important and most measured bio-signal. Moreover, measuring the shape of the arterial pressure pulse allows additional cardiovascular parameters to be assessed, including arterial stiffness.

The main contribution of this thesis is the development of a new method for noninvasive blood pressure pulse monitoring in the upper arm based on using the upper arm brachial artery thickness to radius ratios to determine any variation in blood pressure. The feasibility of the new method of measuring BP will be presented in detail, in addition to adopting its strategies that can make it automatic and easy to perform.

The implemented algorithm is based on the following steps: Initial analysis and feasibility study: in the first phase of the research, the problem is analyzed, the feasibility

of the method that is chosen to be implemented is investigated, and the state of the art is studied.

In particular, the following research will be constrained to:

1. Physiology studies, in particular regarding the cardiovascular system and blood pressure.
2. Research in literature on works concerning the estimation of BP through bio-signals.
3. Studies on the role and utility of microstrip patch antennas in medical applications
4. The scattering transmission coefficient parameter between transmitting and receiving antennas is used to monitor biomedical signals such as blood pressure.

1.2 Thesis Organization

This thesis is organized as follows:

Following the introduction, Chapter 2 presents a comprehensive literature review on the widely available noninvasive methods for measuring blood pressure, complemented by a detailed account of each of them, comparing their accuracy rates and explaining their historical backgrounds. At the end of the chapter, a presentation summary is given on the classification of noninvasive blood pressure measurement devices, their accuracy requirements, and methods of determining accuracy.

Chapter 3 describes the design, construction, and testing of microstrip patch antennas and their use in the detection of blood pressure pulses and noninvasive determination of blood pressure.

Chapter 4 goes on to show the design of the human arm phantom and uses two facing microstrip patch antennas operating at 2.4 GHz, which are placed across interrogated samples. The measured transmission coefficient depends on the change in artery thickness to radius ratios along the signal path, which can be correlated to the intra-arterial blood pressure measurements. There are also some other interesting results related to SAR and source power. The results presented show the relationship between these two measures and their effect on arm tissues.

Chapter 5 presents a potential approach, the pulse transit time for blood pressure measurement. PTT is based on detecting the time delay between the two waveforms of the scattering transmission coefficient variation with respect to brachial artery characteristics variation. Then the work is concluded and compared against the standard Moens- Korteweg equation.

Chapter 6 provides a summary of this work in addition to exposing the proposed work for the remaining thesis.

CHAPTER 2

LITERATURE REVIEW

2.1 Introduction

The objective of this literature survey is to give a general overview of some important aspects of this thesis work. We start by giving a historical overview of the different noninvasive blood pressure measurement methods together with a description of each. Towards the end, we shall show the accuracy of several blood pressure measurement devices.

2.2 What is Hypertension?

Without the pressure that forces our blood to flow around the circulatory system, no oxygen or nutrients would be delivered through our arteries to the tissues and organs [2]. The American Heart Association (AHA) considers normal pressure vital to life [3], and its reading is a systolic pressure of 90-120 millimeters of mercury (mmHg), and a diastolic pressure of 60-80 mmHg, as shown in Table 2.1. The systolic blood pressure indicates how much pressure your blood is exerting against your artery walls when the heart beats [5]. However, the diastolic blood pressure indicates how much pressure your blood is exerting against your artery walls while the heart is resting between beats. [5].

Table 2.1: Healthy and unhealthy blood pressure ranges [2].

BLOOD PRESSURE CATEGORY	SYSTOLIC mm Hg (upper number)		DIASTOLIC mm Hg (lower number)
NORMAL	LESS THAN 120	and	LESS THAN 80
ELEVATED	120 – 129	and	LESS THAN 80
HIGH BLOOD PRESSURE (HYPERTENSION) STAGE 1	130 – 139	or	80 – 89
HIGH BLOOD PRESSURE (HYPERTENSION) STAGE 2	140 OR HIGHER	or	90 OR HIGHER
HYPERTENSIVE CRISIS (consult your doctor immediately)	HIGHER THAN 180	and/or	HIGHER THAN 120

Hypertension, or chronic high blood pressure, is a major public health issue in the United States. It affects 25%-50% of all American adults [3]. Blood pressure (BP) is a vital physiological parameter for the clinical diagnosis and treatment of hypertension, with values varying between systolic blood pressure (SBP) and diastolic blood pressure (DBP) [3-6]. Blood pressure control begins with an accurate measurement, which leads to an appropriate diagnosis and treatment decisions. The hypertensive crisis stage, as shown in Table 2.1, is when the elevated level of blood pressure readings consistently ranges from 120–129 systolic and less than 80 mm Hg diastolic. The second stage is when blood pressure consistently ranges from 130-139 systolic or 80-89 mm Hg diastolic [2]. Third stage: blood pressure consistently ranges between 140-90 mmHg, which can become dangerously high and necessitates immediate medication [2].

2.3 Location of Measurement

The standard location for blood pressure measurement is the brachial artery. Brachial diameter is a useful and simple tool [1]. It should be incorporated into the overall

assessment of cardiovascular (CV) risk, but further studies are warranted to determine the final place of brachial diameter assessment in the routine clinical setting [3][6].

2.4 Previous Blood Pressure Measurement Methods

One of the most important parameters to be monitored and measured in a noninvasive way, but at the same time in a serious and accurate way is blood pressure (BP). Examining BP is vital for clinical review and intervention. Invasive methods are the "gold standard" measurements and therefore the most accurate. The at-home devices are simpler and quicker and require less expertise but are also often less accurate [8]. They also provide in most cases, only one 'snap-shot' measure at a time, while true arterial blood pressure fluctuates continuously. However, they are all sensitive to movement, more expensive and need to be checked frequently for accuracy.

2.4.1 The Auscultatory Method

In fact, the auscultatory at-home devices are noninvasive intermittent techniques [8-9], most common methods currently in use. The at-home devices are simpler and quicker and require less expertise but are also often less accurate [10]. They also provide in most cases, only one 'snap-shot' measure at a time, while true arterial blood pressure fluctuates continuously. The existing devices as shown in Figure 2.1 are a chore: they are cumbersome, finicky, and uncomfortable. The auscultatory method using a mercury sphygmomanometer is regarded as the gold standard for office blood pressure measurement [8-10].



Figure 2.1: Three basic types of blood pressure measurement devices [10]

It uses the detection of Korotkoff sounds by using a stethoscope (a medical instrument for listening to the action of someone's heart or breathing) and a sphygmomanometer instrument to determine blood pressure [10]. This instrument is connected to a column of mercury next to a graduated scale, enabling the determination of systolic and diastolic blood pressure by increasing and gradually releasing the pressure in the cuff [11]. The situation is made worse by the fact that existing aneroid manometers, which use this technique, are less accurate and often need frequent calibration [12]. New devices, known as “hybrid” sphygmomanometers, have been developed as a replacement for mercury devices [12]. Basically, these devices combine the features of both electronic and auscultatory devices such that the mercury column is replaced by an electronic pressure gauge, like oscillometric devices, but the blood pressure is taken in the same manner as a mercury device, by an observer using a stethoscope and listening for the Korotkoff sounds [12]. Most of the auscultatory problems are operator induced with the mercury manometers. That is why, the auscultatory method require annual checks to ensure mechanical wear have not affected readings.

2.4.2 The Oscillometric Technique

To differentiate between office or home settings, many oscillometric devices have been validated that allow accurate BP measurement while reducing human errors associated with the auscultatory approach [10]. With an oscillatory device, a cuff is inflated over the upper arm or wrist to measure arterial blood pressure (BP).

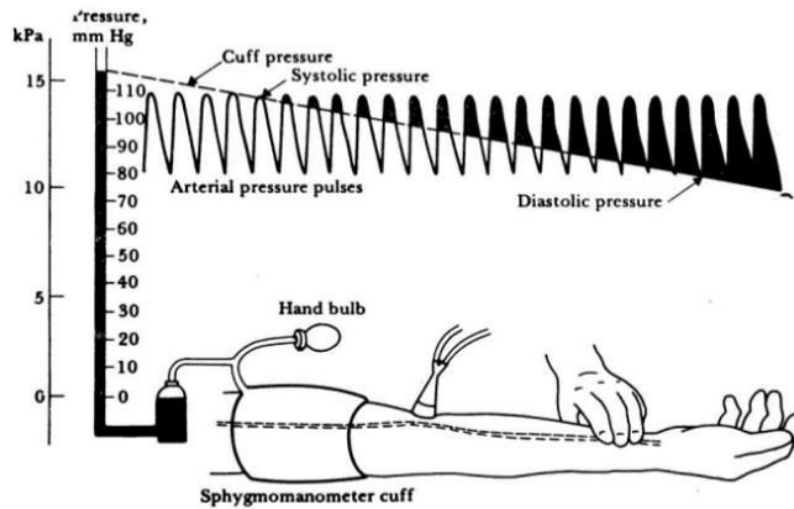


Figure 2.2: Indirect blood Sphygmomanometer measurement [10].

Even when the Korotkoff sounds are hardly detected due to hypotension, the oscillometric method can still monitor BP at regular intervals because the cuff oscillates if arterial pulsation exists [10]. This technique works on the principle of observing the oscillations in the sphygmomanometer cuff pressure as shown in Figure 2.2.

2.4.3 Conclusion

Among the traditional non-invasive methods exposed, the automated sphygmomanometer using oscillometric methods remains the best way to measure BP in terms of safety and usability outside clinics. The advantages of this method are that there is no need to place a transducer over the brachial artery, it presents anti-noise

characteristics, and the cuff can be removed and replaced by the patient during ambulatory monitoring, for example, allowing them to take a shower [9].

Specifically, the volume clamp method [9–10] is based on an inflatable cuff but with a photodiode. These devices need extensive calibration to be accurate. In short, these cuff-based devices permit episodic "snap-shot" measurements of arterial blood pressure while the patient is suspended in a stationary position. A single snap-shot measurement of the time-varying blood pressure, which fluctuates minute-by-minute and from night-to-day, is incapable of encapsulating the dynamic state of the cardiovascular system [9–11]. In addition, these non-invasive methods present discontinuity and discomfort due to the repeated cuff inflations. The methods for measuring blood pressure are categorized in Table 2.2.

Table 2.2: Comparison of the methods of blood pressure measurement [9].

Method	Advantages	Disadvantages	Precision
Catheter	True value, continuous	Invasive	Gold Standard
Korotokoff	Non-invasive	Cuff pressure, sensitive to sound	middle
Oscillometric	Non-invasive	Cuff pressure, sensitive to movement	middle
Tonometry	Non-invasive	Cuff pressure, sensitive to movement	Good
Vascular volume	Non-invasive, continuous	Cuff pressure control	Good
Compensation	Non-invasive, continuous	Cuff pressure control	good

Table 2.2 also lists the advantages and disadvantages of each method. These methods are basically applied when users sit down on a chair with a backrest after a few minutes of calm in a quiet environment such as a hospital or at home [10]. In addition, Table 2.3 lists the difference in precision between each method.

The accuracy of the Tonometry, Vascular volume and Compensation when compared to invasive blood pressure measurement is up to 80%. While the accuracy of compared with invasive blood pressure measurement at the arm or the aorta is quite low to be only 50% to 57%.

Table 2.3: Main error factor of the methods of blood pressure measurement [9,11].

Cause	Error Factor	Systolic BP	Diastolic BP
Measurement Position	Higher than right atrium	Decrease	Decrease
	Lower than right atrium	Increase	Increase
Measurement with cuff	Narrow width	Increase	Increase
	Wide width	Decrease	Decrease
	Wrap loose	Increase	Increase
Measurement method	Slow reducing pressure	Decrease	Increase
	Low hearing ability	Decrease	Increase

2.5 Advances in Wearable Blood Pressure Estimation Technologies

One of the most important parameters to be monitored and measured in a noninvasive way, but at the same time in a continuous and accurate way is blood pressure (BP). Current non-invasive continuous BP monitoring devices including the arterial tonometry method, vascular unloading technique, pulse wave velocity (PWV) method, and pulse waveform characteristic parameter method have several advantages [12-15]. However, they are all sensitive to movement, more expensive and need to be checked frequently for accuracy.

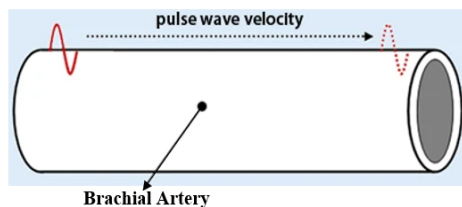


Figure 2.3: Illustrates the pulse wave velocity in brachial artery [15].

Most modern devices still depend on the representation of arterial pulse waveforms from photoplethysmogram (PPG) and electrocardiogram (ECG) recordings. ECG sensors directly measure the change in electrical signals caused by the expansion and contraction of heart activity [16]. Whereas the PPG sensors use a light-based technology to measure the reflected light of the blood volume changes as the heart pumps

[17]. Thus, the PPG can be calculated as the time taken for the arterial pulse pressure wave to travel from the aortic valve to a peripheral site. It is usually measured from the peak of the ECG wave to the peak of the PPG signal, as shown in Figure 2.4.

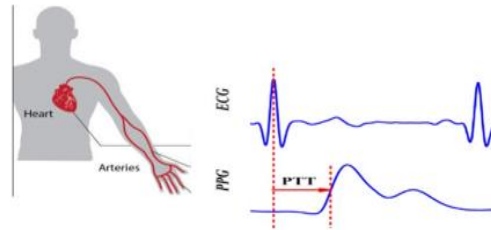


Figure 2.4: The ECG signal and PPG signal. PTT is the difference between the first peak of ECG and first peak of PPG [17].

More recently, attention in one study [17] has turned to wearable radar antennas placed beside each other on the chest. The other PPG and ECG signals are located at the left earlobe and near the sternum in line with the aortic arch, respectively, and are regarded as reference signals to compare the results. However, this device only evaluated systolic blood pressure, whereas diastolic blood pressure is also important in reflecting the amount of pressure in the arteries as the heart relaxes. Yet, the study did not discuss the importance of using radar antennas in identifying important hemodynamic factors and the algorithm used to determine BP. In addition, this system was found to be hard to use and required the patients to be seated quietly.

The relationship describing the propagation of pressure waves in an elastic tube, e.g., a blood vessel, was first described separately by Moens and Korteweg in 1871 [17,18]. The BP estimation method based on Pulse Transit Time (PTT) is of great evaluation because it can offer a cuffless and comfortable long-time BP measurement with no risk to the patient [17,18]. It has received considerable attention for noninvasive cuffless blood pressure measurement. The PPT is the measure of the time interval

necessary for the pressure pulse to spread into peripheral blood vessels. It begins when the pulse pressure is detected in the aortic vessel due to the systolic phase of the heart cycle, and it finishes when the pulse is detected in the distal part of the vessels [19,20].

The common PTT-BP measuring method requires at least two simultaneous signals, such as an electrocardiogram (ECG) and a pulse wave, which is hard to deploy in wearable devices for cuffless and continuous BP estimation [20]. Therefore, cuffless BP measurement based on a one-channel pulse wave is more effective to reduce the complexity and inconvenience of PTT-based methods.

Existing blood pressure estimation methods based on pulse wave velocity rely on measurement of pulse transit time (PTT) [20,21]. Their relationship is given in (2.1).

$$PWV = \frac{L}{PTT} = \sqrt{\frac{E \cdot h}{2r\rho}} \quad (2.1)$$

where L is the vessel length, ρ is the blood density, r is the inner radius of the vessel, h is the vessel wall thickness, and E is the elastic modulus of vascular wall [21]. The elastic modulus E is given by the Hughes equation:

$$E = E_0 \exp(\zeta P) \quad (2.2)$$

In equation 2.2, E_0 is the elastic modulus at zero blood pressure, ζ is a material coefficient of the artery, and P refers to BP. Many of the previously reported relations between blood pressure and pulse wave velocity present only empirical algorithms without any realistic assumptions about human arteries. The most popular ones are Moens-Korteweg (MK) [22] and Hughes Equations. The Moens-Korteweg (MK) [Bramewell] + Hughes Equations [Hughes] are generally used to relate PWV to the blood

pressure P [22,23]. These two equations are considered as the BP varies; the thickness/radius ratio remains fixed. In addition, the artery wall remains thin in response to these variations.

The difficulties associated with using pulse wave velocity to estimate BP can be divided into two general categories:

1. Inaccurate measurement of PWV using non-invasive sensors.
2. Employing static calibration equations to map the PWV measurements to BP.

Although PTT provides a good estimate of BP and has been considered a promising surrogate for noninvasive continuous BP monitoring. There are some limitations to the PTT method. PTT-BP models should be performed at the measurement lab, and they must be repeated every 2–5 minutes [22-24]. Some of them provide the mean PWV for each segment and, thus, an independent determination of systolic and diastolic BP, referred to as either SBP or DBP, respectively. After several intervals of intermittent measurements, this tool most importantly requires re-calibration for accurate measurements. All these challenges put this method under investigation. Using arterial cross-sectional area or diameter parameters may easily solve the pulse waveforms. Thus, the possibility of using the PTT method along with the transmission coefficient waveform analysis can obviously produce a suitable outcome in detecting different vascular diseases.

Recently, researchers are focusing on electromagnetic (EM) wave sensing and microstrip patch antennas as leading technologies due to their interactions of scattering, reflection, absorption, and transmission inside the human body that allow specific physiological features such as blood pressure to be determined. The microstrip patch

antennas are metallic sensors that can radiate and receive EM waves [7]. The properties of the reflected and transmitted waves, in terms of scattering parameters (S parameters), are used to analyze and determine the BP levels. S parameters are defined as the input-output relationship between the terminals of the EM sensors.

In [23], the authors developed a low-cost wearable piezoelectric-based system to validate a straightforward computation for continuous beat-to-beat blood pressure measurement. The method needs no calibration as it uses the summation of initial blood pressure and pressure change without the need for calculating correlation. The initial blood pressure change in the radial artery was extracted by systolic and diastolic feature points in the pressure pulse wave (PPW) [23]. Figure 2.5 depicts the created system, which is made up of three primary components: a piezoelectric sensor, a front-end analog circuit, and a software processing unit.

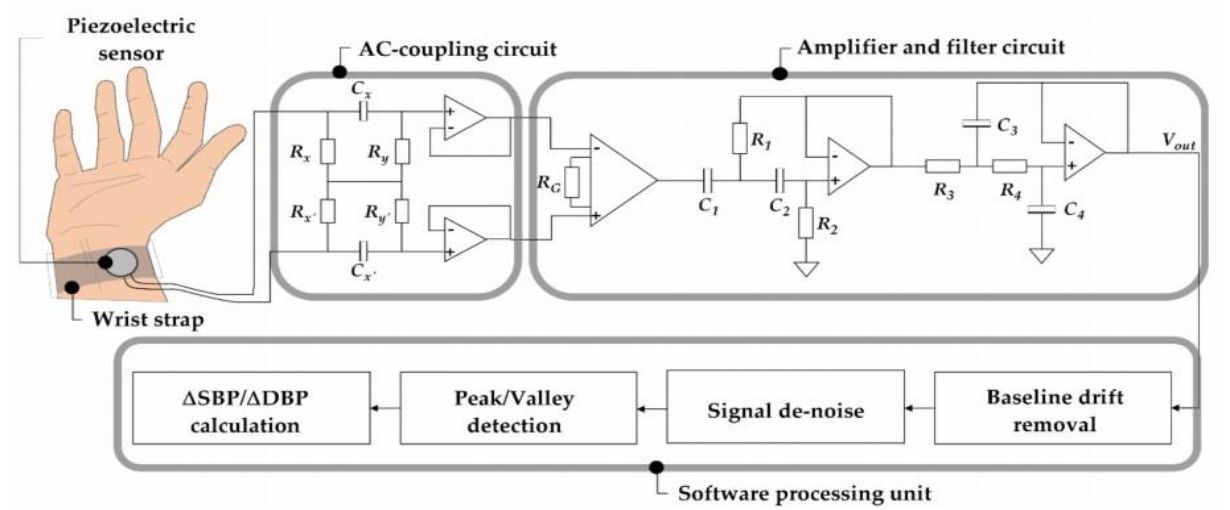


Figure 2.5: Schematic of the overall system [23].

This sensor detects any blood pressure variations that can transform the pressure signals into electric signals via the pressure sensitivity [23]. Finally, the software-processing unit is responsible for detecting systolic and diastolic blood feature points and

then calculating the pressure changes between the adjacent waves. They relied on a straightforward method to convert voltage changes to pressure changes in PPW signals directly via piezoelectric properties of pressure sensitivity. However, stable PPW signals from the radial artery remain a significant issue that can also be affected by daily activities such as muscle changes caused by walking, eating, dressing, grabbing, etc. No doubt, the solid structure of the piezoelectric sensor could easily induce air gaps under extended use during daily activities. Furthermore, to make this method more trustworthy, this strategy requires enhanced analog frontend construction in ambulatory blood pressure monitoring, as well as more participants, particularly individuals with blood pressure difficulties.

Accordingly, [24] focused on designing two transmit and two receive antennas in parallel for the purpose of a non-invasive, continuous blood pressure estimation method. The continuous radar works by sending and receiving EM signals out of the continuous radar for pulse wave analysis. Yet, these antennas need further optimization as they were not designed to transmit and receive signals from the human body.

Zhao et al. [25] presented a continuous Doppler radar device from which beat-to-beat BP can be calculated. The main limitation with this device was that the person must be in a seated position and the wave radar must be 0.5 m away from the body, which is not feasible for continuous wearable body devices [25]. Furthermore, Woo et al. [26] reported a non-invasive mechanism of tissue equilibrium absolute pressure measurement. This mechanism is embedded in a wearable watch type measurement module for continuous BP tracking, but low accuracy for BP reading limits the use of this device.

Lin and colleagues developed a novel nanosecond pulse nearfield sensing (NPNS)-based screening technology with dual antennas in [27]. Their project is based on a miniature transceiver that transmits radio frequency (RF) pulse transmission using two

combined flat antennas. Their project is to derive relative blood pressure parameters from measured blood flow activity. These blood parameters, including pulse wave velocity (PWV), average systolic and diastolic times, are obtained by dedicated software for clinical and homecare applications. The architecture of the transceiver is presented in Figure 2.6, and is composed of a transmitter, a receiver, dual antenna, signal processing, and a display part.

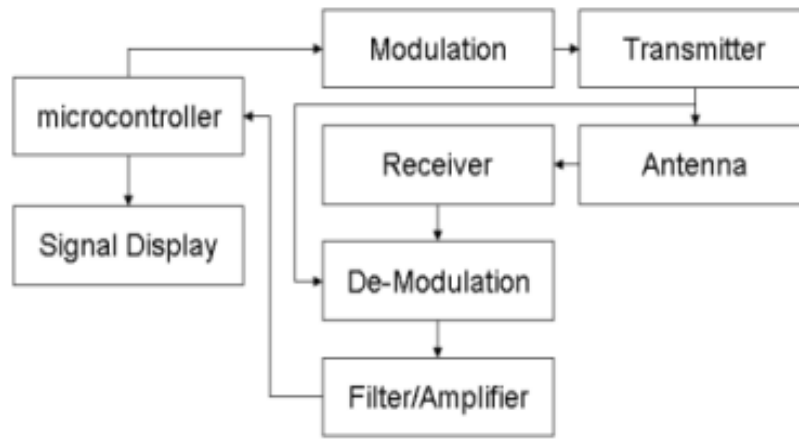


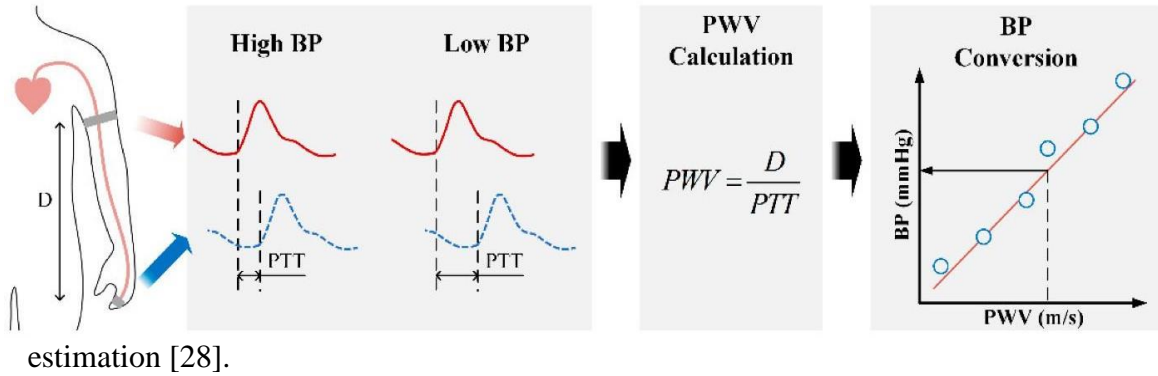
Figure 2.6: Architecture of proposed NPNS based radar system for artery pulse signal detection [27].

The radar is based on multiplication of reflected and reference RF pulse signals. The output signal of the correlation system is proportional to amplitude and phase difference between those signals. The size of the ready to use and previously designed NPNS device is $10 \times 3.5 \text{ cm}^2$. This system designed is dedicated for sensing, signal processing and wireless data transmission in a non-contact and non-invasive way for personal healthcare.

The researchers in [28] presented an accurate, small-sized bioimpedance measurement system for blood pressure monitoring that was tested on different human body areas. The bioimpedance measurement system continuously reflects the change in BP through the change in the arterial cross-sectional area, which is monitored by the

change in arterial impedance as described in Figure 2.7.

Figure 2.7: Methodology of pulse wave velocity (PWV)-based blood pressure (BP)



The bioimpedance measurement system developed by authors in [28] works by injecting a small electric current (500 μ A) into the human skin. This method monitors the change in skin impedance by voltage measurement using two pairs of electrodes, as shown in Figure 2.8. In hardware implementation, an ultra-low noise amplifier with a 40 dB high gain is used to detect any small variation in arterial impedance. Then a band pass filter with cutoff frequencies of 0.1 Hz to 3 Hz is applied to remove any noise and provide a clear signal.

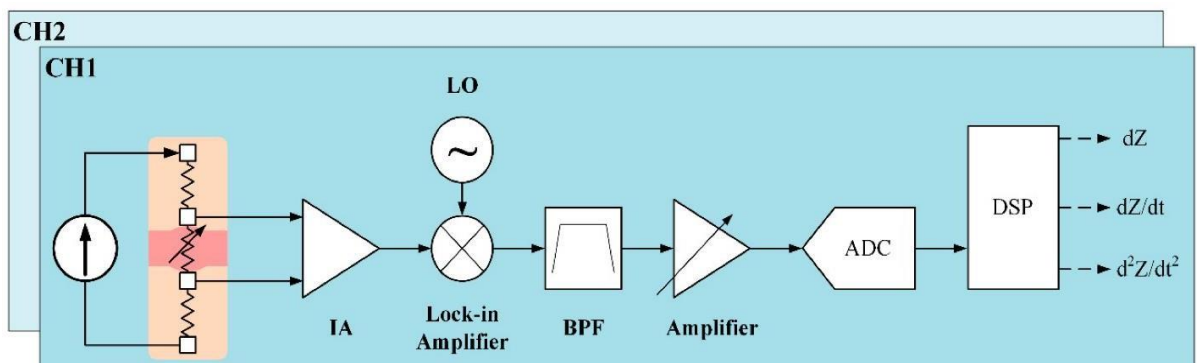


Figure 2.8: System Design [28].

The two bio-impedance channels (BI) are used to assess the pulse wave velocity (PWV) values. The efficiency of these BI channels is compared to a commercial pulse sensor. In summary, the proposed design provided good tracking of BP variations (PWV and PTT) but with high power consumption in comparison to previous commercial pulse pressure sensors for the same level of accuracy.

2.6 Effect of Exposure of Electromagnetic Radiations on Human Body

Previous research is investigating the effects of being exposed to electromagnetic waves inside or on the surface of the human body as we are exposed to this radiation daily. The biological reaction under the exposure of an electromagnetic field is of great significance while designing and developing a system. Therefore, it is important to note and identify the biological interaction between human tissue characteristics and EM waves, in which these EM waves exhibit ionizing, and non-ionizing radiation classified by frequency [29-32]. In this manner, the authors [33] studied the effect of electrical and electromagnetic fields on human bone repair. Their preclinical experiments revealed that EMF waves can promote and regulate the synthesis of bone healing molecules. Furthermore, the scientists in [34] studied the effect of electrical and electromagnetic fields on human bone repair.

The authors in [34] related the characteristics of biological tissues when dealing with the propagation of ionizing electromagnetic energy for the treatment of different tumors. It is found that electromagnetic energy absorption is different for each tissue. The given study considers the high exposed frequency the more electromagnetic penetration characteristics of the fat and blood rather than bone and fat. As a result, the lower the frequency to which the human body is exposed, the safer it is.

Non-ionizing radiation is described as a series of energy waves composed of oscillating electric and magnetic fields traveling at the speed of light [31,32]. Non-ionizing radiation is classified according to its frequencies from 0 Hz to 1.1 THz, including the spectrum of ultraviolet (UV), visible light, infrared (IR), microwave (MW), radio frequency (RF), and extremely low frequency (ELF). Many studies [34,36] have examined the association between non-ionizing EMF exposure and considerable health risks to potentially exposed workers if not properly controlled. Because the waves do not penetrate deep directly into the tissues, this non-ionizing radiation is eventually found to be safe in the application of biomedical devices used in most EM diagnosis and therapeutic modules.

On the other hand, in 2015, the European Commission Scientific Committee on Emerging and Newly Identified Health Risks [35] reviewed the epidemiologic studies of extremely low frequency fields and found that these studies had shown an increased risk of childhood leukemia with estimated daily average exposures above 0.3 to 0.4 microTesla (T), although no mechanisms have been identified and there is no support from experimental studies that explains these findings. So, exposure to intense and direct amounts of non-ionizing radiation may result in damage to tissue due to excess heat [34]. This is only common for those who work on large sources of non-ionizing radiation devices. The heating effect on the tissue is normally quantified by the Specific Absorption Rate (SAR) [35-37]. In [37], the authors investigated the hazardous effects of electromagnetic radiation from a source on the human body. They consider the signal efficiency of the implemented wireless medical devices and their safety SAR level guidelines for radiation exposure. Different power levels are set for users of different body sizes. It has been shown that almost all the radiated power is absorbed by the human

body. This led to the importance of reducing the input power of these medical systems so that the radiation harm absorbed by the human body is reduced. To date, only clinical studies can relate to adverse health effects in response to EMF exposure.

The Specific Absorption Rate (SAR) tool, which is expressed in watts per kilogram of body weight, measures the rate at which energy is absorbed by human tissues [37]. In other terms, it is a measurement of how much power is absorbed per unit mass of a conductive material and is defined as:

$$SAR = \frac{\sigma |E|^2}{\rho} \quad (4.1)$$

where σ is the electrical conductivity of the material, E is the RMS magnitude of the electric field at a given point and ρ is the mass density of the material [37]. Thus, SAR measures exposure to fields between 100 kHz and 10 GHz.

CHAPTER 3

FLEXIBLE WEARABLE MICROSTRIP ANTENNA FOR SKIN CONTACT APPLICATION

3.1 Theoretical Equations

To improve upon the current devices, it is critical to apply the concept of electromagnetism to the existing medical devices and to explore appropriate antenna design, performance, radio frequency settings, power utilization, and safety. Modeling the physiological system and applying the wearable antenna properties to the model can help with some of this.

Medical applications working at industrial, scientific, and medical radio band frequencies (ISM frequency range: 900, 2400, and 5000 MHz, respectively), usually utilize flexible antenna substrates of commonly low dielectric constants that are powerful, lightweight, and can withstand mechanical strains [38]. The main challenges in the design and implementation of the on-body adaptable antennas are the proper selection of a low-loss dielectric substrate material, compact size, and simple antenna shape [39].

The width of the proposed microstrip patch antenna can be calculated as follows [7]:

$$W = \frac{C}{2 \cdot f_0 \sqrt{\frac{\epsilon + 1}{2}}} \quad (3.1)$$

Where W is the width of the patch, C presents the speed of light, f_0 presents the operation frequency, and ϵ presents the value of substrate permittivity.

Because the permittivity of the air and the dielectric substrate differs, the value of the effective dielectric (ϵ_{eff}) is computed using equation 3.2.

$$\epsilon_{eff} = \frac{\epsilon + 1}{2} + \frac{\epsilon - 1}{2\sqrt{1 + 12\frac{h}{W}}} \quad (3.2)$$

The value of (ϵ_{eff}) the dielectric constant of air stays between 1 and the dielectric constant of the substrate (ϵ_r), because the electromagnetic fields excited by the microstrip resides partially in the air and partially in the substrate [7]. Now, as operating frequency increases, the effective dielectric constant (ϵ_{eff}) increases and eventually approaches the value of the substrate dielectric constant (ϵ_{eff}).

$$\Delta L = 0.412h \left(\frac{\epsilon_{eff} + 0.3}{\epsilon_{eff} - 0.258} \right) \left(\frac{\frac{W}{h} + 0.264}{\frac{W}{h} + 0.8} \right) \quad (3.3)$$

Also, due to the fringing effect, the electrical length of the patch increases by $2\Delta L$ [7].

$$\Delta L = L + 2\Delta L \quad (3.4)$$

With no adverse effects noted, our proposed model uses the transmitted and reflected EM waves from a wearable antenna to analyze and determine the input-output relationship between terminals of EM sensors. One major problem with utilizing antennas lies in the lack of safety and SAR test limit determination either on phantoms or on real

human bodies. The main goal of the current work is to provide a groundwork simulation and measurement model to potentially correlate the scattering parameters obtained from a microstrip patch antenna placed on the human arm phantom for estimation of blood pressure. The relationship between blood pressure and brachial artery radius will be explored utilizing a simulated human arm model, including the brachial artery and arterial thickness variation.

3.2 Methodology

3.2.1 Flexible Antenna Geometry

This thesis presents a non-conventional microstrip antenna that can be placed in contact with the human skin for biomedical applications. The unique operating environment of wearable antennas, i.e., on human body, impose additional requirements in the design phase of the antennas. Reducing the size and complexity of the antennas used in these applications has been the primary objective of recent antenna research [39-43].

The antenna is inspired from the literature [41,42]. It is of compact rectangular microstrip line-fed antenna with a $50\ \Omega$ microstrip feed line and a waveguide (partial ground plane, substrate and radiating patch). The conventional patch antenna was designed and optimized in an ANSYS HFSS environment.

Although the microstrip antenna implemented in [41,42] is flexible and dedicated for medical applications, the resonant frequency achieved in free space and with no curvature is 2.3 GHz. On the other hand, the proposed antenna is proved through simulation and measurement to attain a resonant frequency of 2.4 GHz. This is achieved as shown in Figure 3, by truncating both sides of the antenna, creating a hole at the center

and changing the substrate material resulting in resonance at the targeted frequency of 2.4 GHz. The proposed antenna geometry as shown in Figure 3.1, achieves a narrow band with good matching properties at 2.4 GHz. The narrow band radiator antenna focusses its power on the signal of interest while tuning out any interferences. Moreover, the receiving antenna can cancel out unwanted wideband noise [41,42].

Indeed, the full ground plane in the initial design is replaced by a partial ground plane, in order to shift resonance from 2.2 GHz to the targeted ISM frequency of 2.4 GHz and maintains a narrow band. Thus, the designed antenna is small in size, robust, low cost, consumes a small amount of power, comfortable to wear and is easy of manufacturing. Such antenna geometry is suitable for body-worn applications.

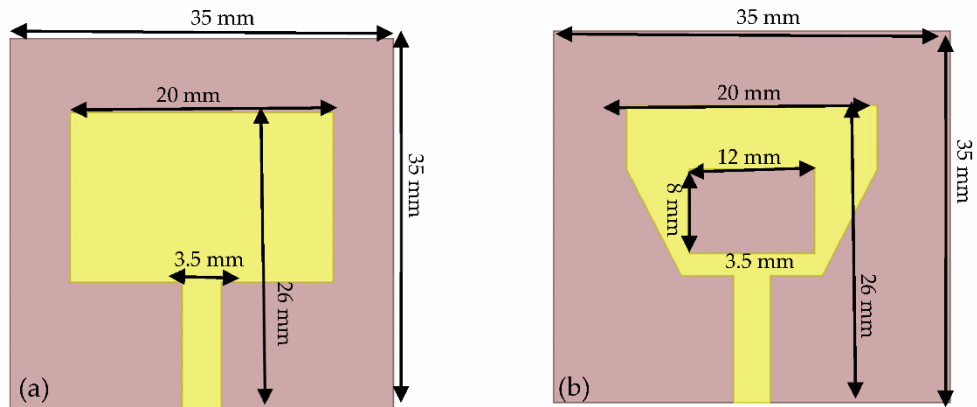


Figure 3.1: (a) Conventional microstrip patch antenna versus (b) the proposed patch antenna.

A parameter sweep simulation was performed by changing the width of the slot from 6 mm to 12 mm and at the same time changing the length of the slot from 2 mm to 8 mm, resulting in four steps. Results suggest a clear trend: both the resonant frequency and the reflection coefficient magnitude are displaced due to an decrease in slot width, as shown in Figure 3.2. The simulated $|S_{11}|$ results for the four pattern configurations are shown in Figure 3.2.

It was observed that the use of a patches, with a slot inside the patch along with truncated corners at a 60-degree angle, can lead to an optimized design that sufficiently with attractive S11 frequency response.

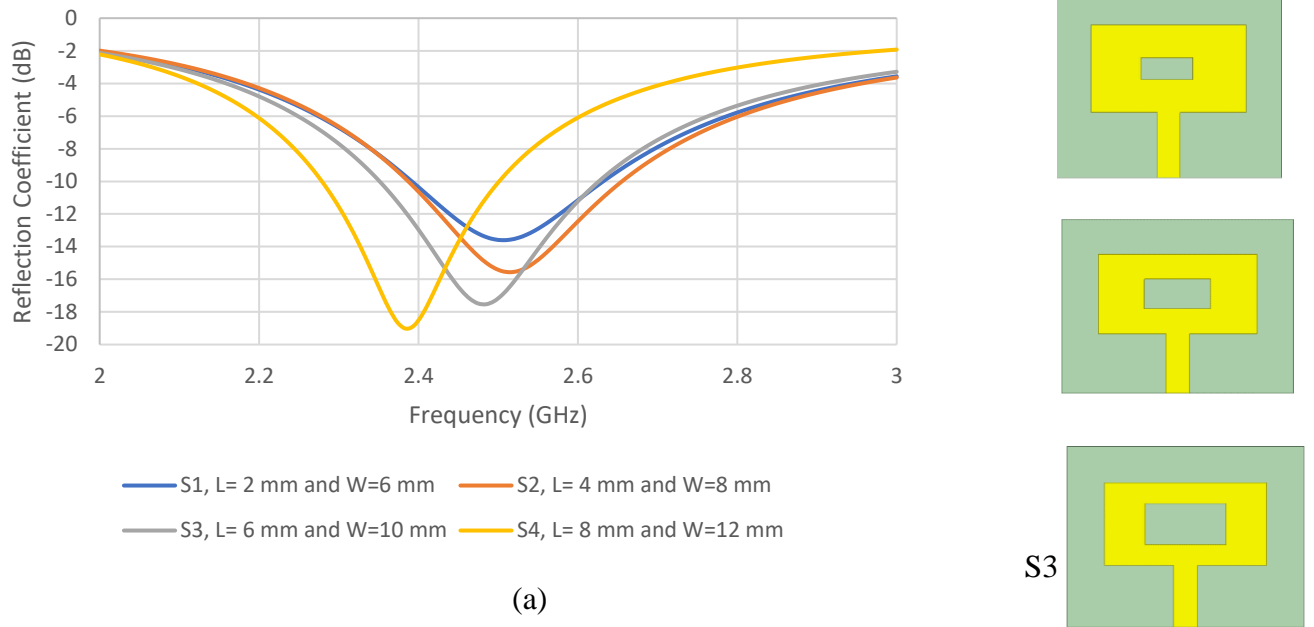


Figure 3.2: The simulated parametric analysis on the length and width of slot of the proposed antenna.

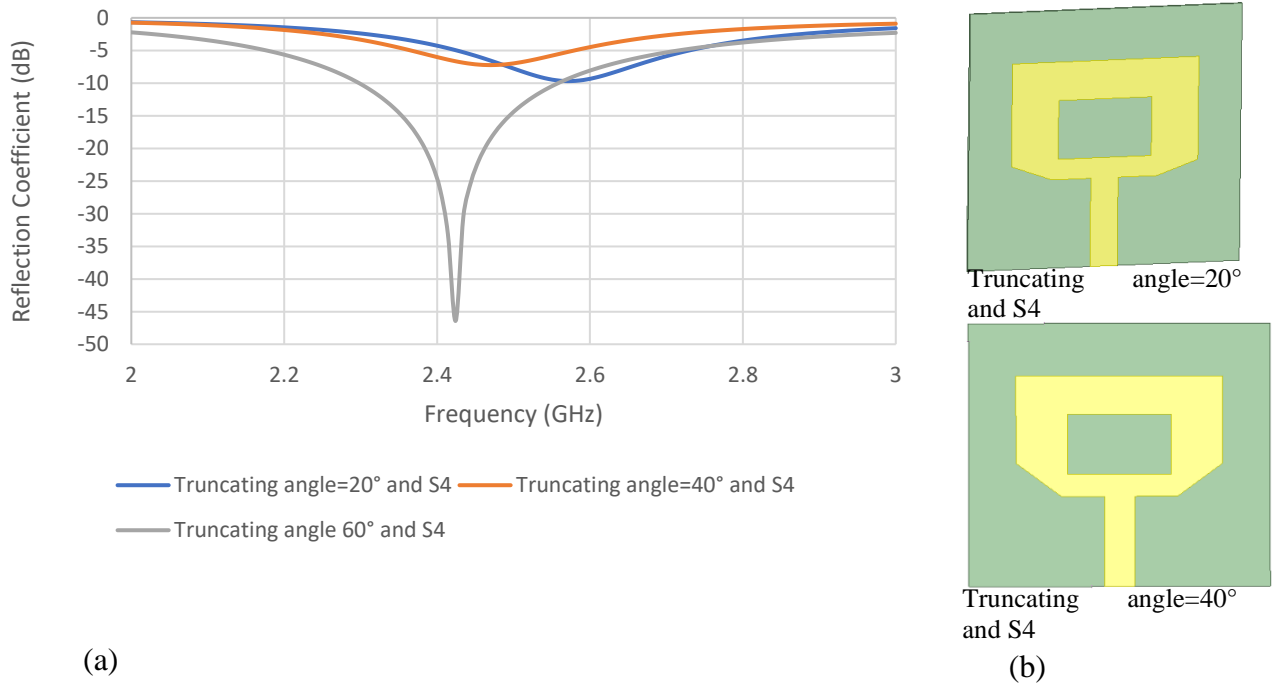


Figure 3.3: (a) Optimizing antenna performance based on three truncating angles along with a slot inside the patch. (b) shows the geometry of the truncated-corner patch.

Antenna dimensions were optimized, as shown in Table 3.1, according to the theoretical design rules mentioned before.

Table 3.1. Optimized dimensions of the simulated patch antenna parameters.

Parameter	Value (mm)
Ls	35
Ws	35
Lp	26
Wp	20
Lg	35
Wg	4

Ls: Length of substrate; Ws: Width of substrate; Lp: Length of patch; Wp: Width of patch; Lg: Length of ground plane.

The epoxy substrate was of 0.4 mm thickness (h), of 35×35 mm area, and the dielectric constant and dielectric loss tangent were $\epsilon = 4.3$ and $\tan\delta = 0.004$, respectively. Epoxy substrate was utilized as it can be used across curved surfaces. The schematic of the proposed antenna is shown in Figure 3.4.

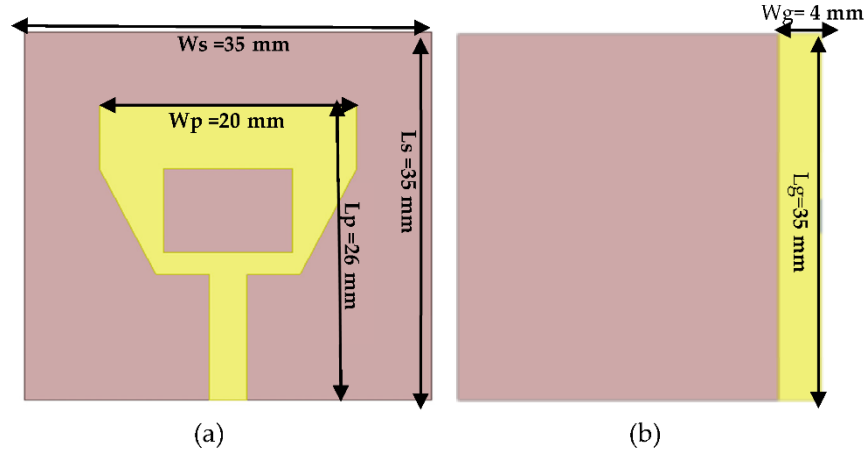


Figure 3.4: Designed flat patch antenna on epoxy flexible material: (a) front view and (b) bottom view.

The antenna operating at 2.4 GHz, exhibits high gain, high directivity, good electrical efficiency and noticeable detection range.

Table 3.2. Comparison of the proposed antenna to the antenna provided in literature.

Specifications	Novel design	Literature
Operating Frequency	2.4 GHz	2.45 GHz
Size (mm^2)	35x35	24x28
Power Consumption	50 mW for two pairs of antennas	1 mW for one antenna
Substrate	Epoxy	Rogers Duroid RO3003™
Thickness of Substrate (mm)	0.4	1.52
Simulated human arm	Close to real human arm	Rectangle human arm

Note that the antenna described in the literature if re-designed with the same specifications provided, the operating frequency is about 2.3 GHz.

The proposed design antenna is set to be of flexible substrate of low thickness compared to the one provided in the literature. The flexible epoxy substrate utilized, is said to be conformal to the surface, can be used across curved surfaces and can be

integrated into flexible electronic systems for wearable applications. Patch size was chosen such as the antenna operates at 2.4 GHz.

3.2.2 Antenna Simulation in Bending Condition

For wearable applications, when an antenna or sensor is placed on the human body, there is a greater probability that the platform where the antenna is placed is not flat. Moreover, the antenna can bend at different angles because of human movement. Hence, a compact, flexible antenna is needed that can operate well at certain bending angles.

Figure 3.3a, b compares the fabricated planar antenna using a coaxial feed to the bent antenna over a cylindrical shape with different radii, which also accommodates different human curvatures. As shown in Figure 3.3c, the antenna is measured in free space as a reference, resulting in a reflection coefficient (S_{11}) of -45 dB at 2.42 GHz with a high radiation efficiency.

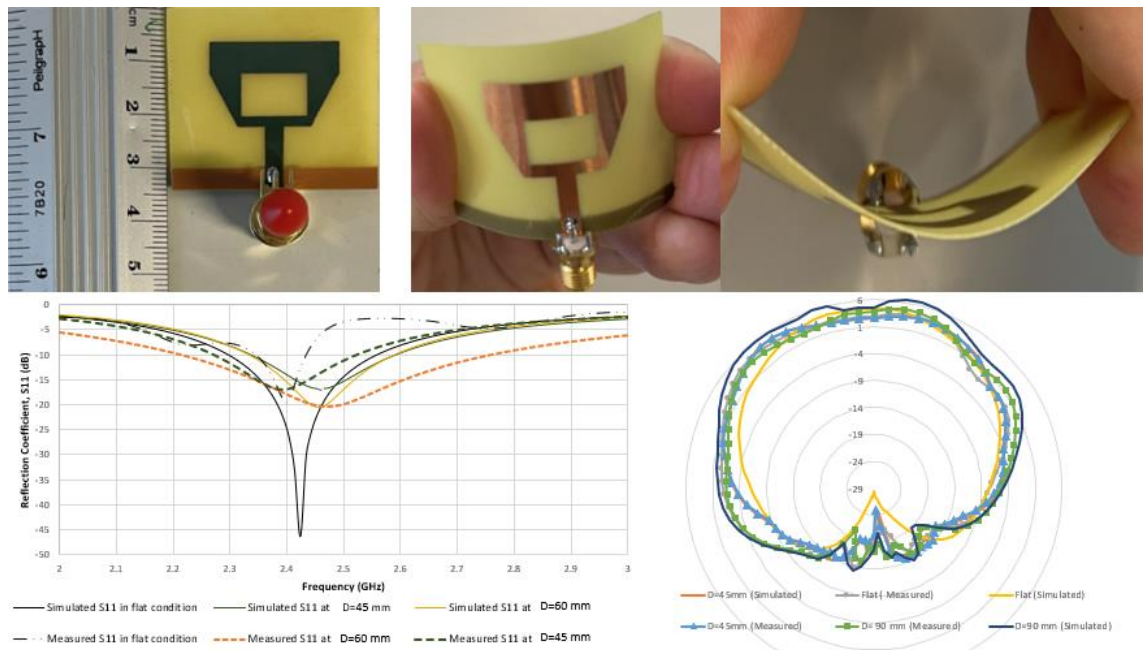


Figure 3.5: Structure and performance measurement of the fabricated patch antenna: (a) schematic of fabricated antenna with coaxial feed on a flexible substrate; (b) photos of different antenna bending around cylinder of diameter 45mm and 60 mm; (c) variation of measured (dotted lines) and simulated (solid lines) reflection coefficient for different bending diameters; (d) simulated and measured off-body 2-D radiation patterns at 2.4 GHz of the proposed antenna in flat and at different bending conditions.

The antenna operating at 2.4 GHz, exhibits high gain and good electrical efficiency.

Generally, a larger return loss results in more energy delivered into the antenna. As discussed previously, the effects of bending flexible antennas have an impact on radiation characteristics such as resonant frequency, reflection coefficients, and gain. The impact on the S -parameters, which indicates the percentage shift, or the deviation, of the resonant frequency and the loss of signal strength because of the impedance mismatch and thus the creation of the surface waves. Yet, the antenna still operates under normal conditions since S_{11} is below -10 dB.

A more detailed cartesian plot of the radiation pattern to show the differences between flat and bending diameters is shown in Figure 3.6.

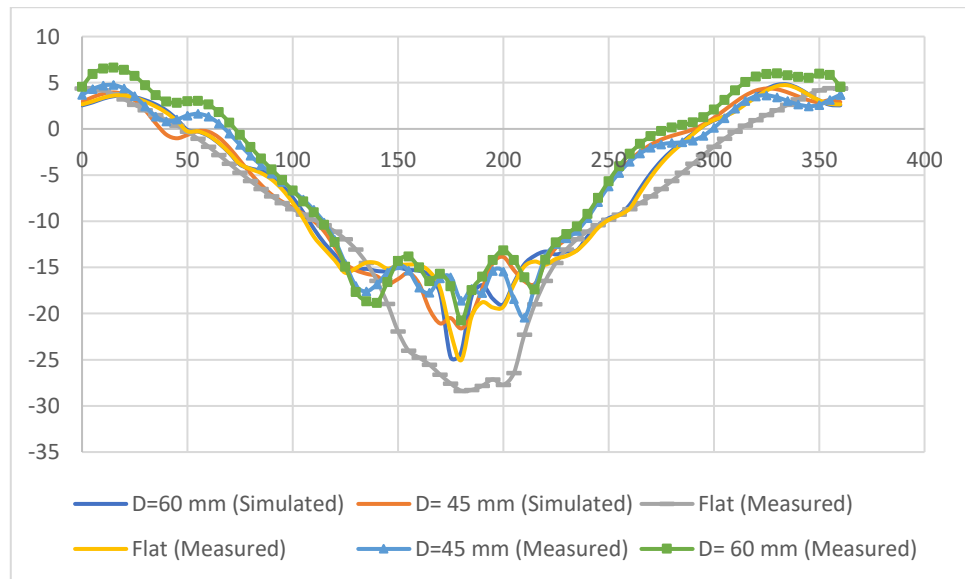


Figure 3.6: Cartesian plot of the radiation patterns between flat and bending diameters.

Table 3 shows the increment of return loss (S11) as the bending increases; that is as a function of the diameter.

Table 3.3. Change in radiation characteristics of antenna with bending.

Cylindrical Bend [mm]	Reflection Coefficient [dB]		Bandwidth (GHz)	
	Simulated	Measured	Simulated	Measured
D=0 at 2.4 GHz	-47	-20	0.25	0.15
D=45 at 2.15 GHz	-17	-13	0.2	0.25
D=60 at 2.4 GHz	-17	-19	0.25	0.22

3.2.3 Transmit/Receive Antennas in Free Space

To determine the transmission coefficient scattering parameters of antennas, two microstrip patches were fabricated and placed 6.25 cm apart in free space as shown in Figure 3.5.

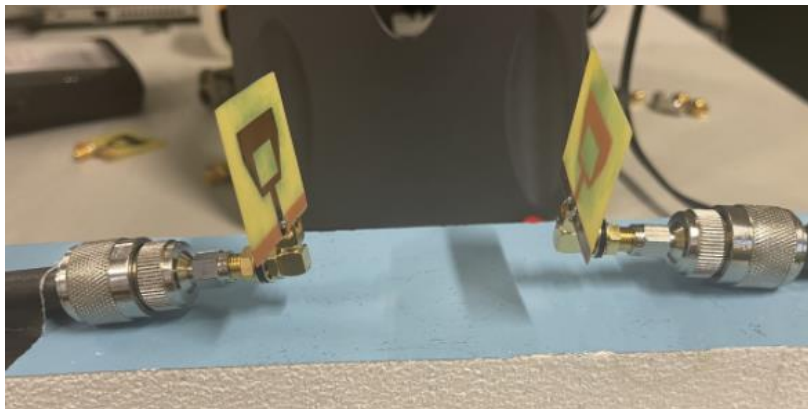


Figure 3.7: Two fabricated antennas in free space separated by 6.25 cm.

The distance must be at least a half wavelength to avoid mutual coupling [7].

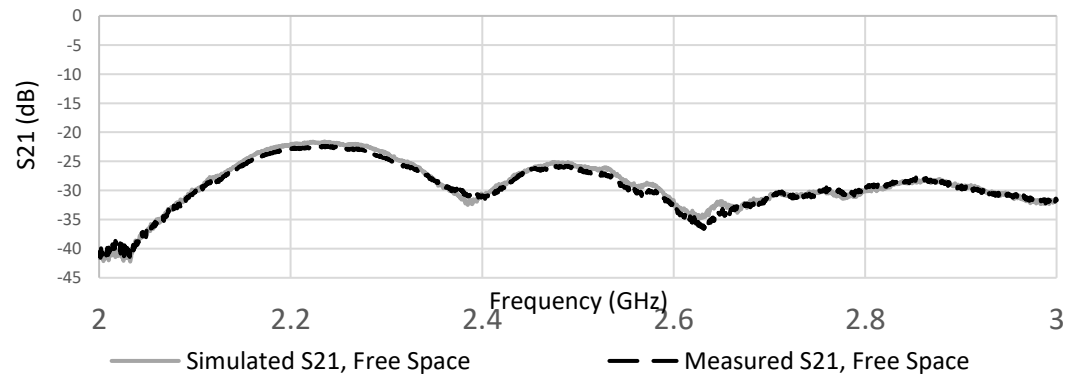


Figure 3.8: Simulated versus measured transmission coefficient between two antennas in free space.

CHAPTER 4

DESIGN OF HUMAN ARM

4.1 Human-Tissue-Arm Equivalent Simulated Phantom Modeling

One of the challenges in simulated phantom development for wearable antenna testing is the fact that the human arm is a heterogeneous medium with layers of different tissues with different permittivities, as shown in Figure 4.1. The variation of dielectric constant with frequency range allows reaching the targeted veins and arteries, through the skin, muscle, bone, blood and fat tissue layers while maintaining good sensitivity. This variation impacts the acquired signal and also affects the sensing brachial artery wall thickness to vessel radius ratio (h/R).

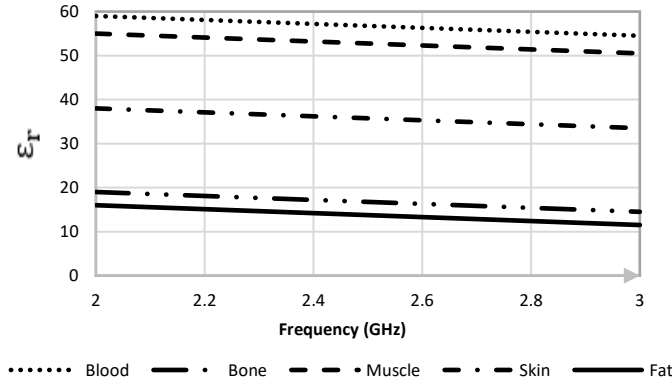


Figure 4.1: Relative permittivity (ϵ_r) in the frequency range from (2-3) GHz of the biological tissues selected for the heterogeneous simulated samples.

To define the 3D model arm, it is necessary to define the characteristics of the different arm tissues in HFSS. HFSS requires the mass density, the conductivity, the relative permittivity, and the loss tangent of each of the tissues at any specified frequency. The Foster website [45] provides tissue parameters across the entire frequency range.

Table 4.1 provides the electromagnetic properties of human body tissue layers at 2.4 GHz. It clearly shows that the blood has the highest permittivity, whereas fat and bone have similar permittivity. It also presents the different electrical permittivity (ϵ_r) and conductivity σ (S/m) properties in addition to the different mechanical compressibility σ_{mec} ($W/K/m$) and the mass density ρ (Kg/m^3) properties of each tissue at 2.4 GHz [46,47].

Table 4.1: Dispersion characteristics of human tissue layers at 2.4 GHz.

Tissues	ϵ_r	σ (S/m)	ρ (Kg/m^3)	σ ($W/K/m$)
Skin	40.93	0.89	1100	0.293
Fat	5.34	0.08	1100	0.201
Muscle	55.19	1.49	1850	0.46
Bones	12.36	0.15	1020	0.41
Blood	59.19	2.11	1000	0.505

σ (S/m): conductivity

ρ (Kg/m^3): mass density

σ_{mec} ($W/K/m$): mechanical compressibility

As shown in Figure 4.2, a six-layer model (skin, fat, muscle, bone, artery, and blood flowing inside the artery) has been considered for the evaluation. The simulated arm model is developed in ANSYS HFSS. It simply represents a portion of the human body; that is, the upper arm. When conducting electromagnetic simulation tests for wearable antennas, this simulated implementation model is found to be cheaper and less complex than the voxel model, which is capable of capturing a high-resolution degree of anatomical detail.

The fat layer has a thickness of 3 to 6 mm, and the muscle layer has a thickness of 10 to 15 mm from the axis. The artery is reasonably modeled to mimic the brachial artery blood properties, for which simulation has been performed using seven different diameters: 4.3 mm, 4.4 mm, 4.5 mm, 4.6 mm, 4.7 mm, 4.8 mm, and 4.9 mm, as also reported by some previous works [48-52]. Thus, the choice of different arterial diameters changing uniformly at a long frequency range compromises the characteristics of the arterial system.

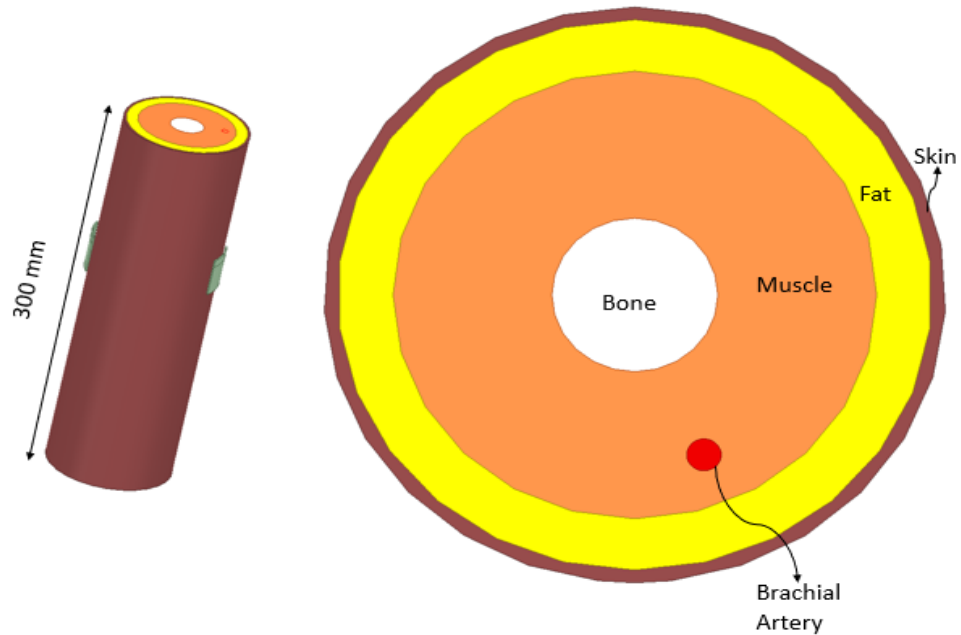


Figure 4.2: Cylindrical modeled multi-layer human arm model developed in ANSYS HFSS, (a) perspective view, (b) cross section of the top view (zoomed in).

Blood as a biological tissue does possess high permittivity and conductivity over the frequency range, it does possess significant changes in the overall behavior of this work.

The small diameter increase constitutes the response in a healthy brachial artery. It is found that the maximal brachial artery diameter was 4.90 mm, and the early minimum diameter was 4.33 mm [50].

4.2 Specific Absorption Rate (SAR) Analysis vs. Power of an Average Simulated Human Arm Phantom

The arm is a complex part of the body to simulate because it has multiple layers of different tissues. Regarding the short distance between arm tissues and the EM fields, it might also be the most affected body part by the antenna radiation. As a result, the arm has been simulated in this project to estimate the potentially harmful effects of electromagnetic field interaction with biological tissues on health. In the same field, antenna radiation has an adverse impact on human body tissue. Therefore, the existence of the human body has to be taken into consideration during the design simulation and, most importantly, during the experimental validation of the wearable antenna. This is because wearable antennas can emit electromagnetic fields, which in turn interact with human body tissues.

As explained before, HFSS software provides a SAR calculator. It is a particularly useful tool that allows calculating SAR in tissue volumes. For the distress signal frequency, the range of source power simulated has been from 1 W to 50 mW. In order to know how the SAR levels of the arm tissues change depending on the source power, the simulations performed at 2.4 GHz have been repeated, changing the power source each time.

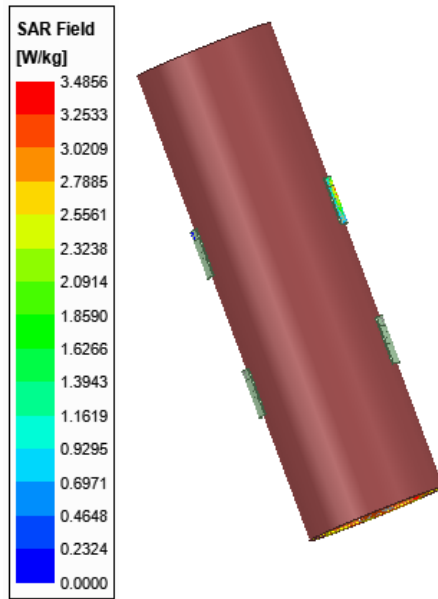


Figure 4.3: The peak 10g SAR value at the surface of the arm.

During the simulations, it was observed that the blood and the skin absorbed more energy than any other tissue as shown in the below Figure.

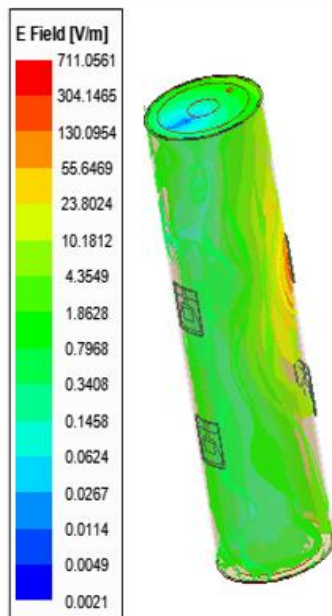


Figure 4.4: Simulated total electric field strength at the absorbing conditions.

Since the density and conductivity of bone are low, it has the least energy

absorption of the tissues. For an input power of 1W, the average SAR value is high compared with the SAR limit in the U.S. Thus, the input power must be decreased for the SAR values to decrease. Simulations for a 10 g average specific absorption rate (SAR) based on IEEE-Standard for a human arm at different input powers were also carried out. The safest input power was 50 mW with an acceptable SAR value of $3.89 \text{ W/Kg} < 4 \text{ W/Kg}$ as listed in Table 4.3. There is no doubt that the skin is the most affected tissue. In fact, low SAR levels are critical to this study since the antennas have continuous exposure to radiation waves that go deep inside the human arm.

Table 4.2: Simulated SAR in one gram and ten grams of arm tissue obtained from HFSS for the antennas placed at both sides of the human arm.

Power (mW)	SAR for 10 g (W/Kg)
1000	1.4917×10^3
800	1.1933×10^3
600	25.222
400	16.334
200	10.089
100	5.044
50	3.89

First, at this frequency, all the tissues have a linear relation between SAR and source transmitting power. This is due to the fact; power is proportional to the square of the electrical field. SAR is equal to the square of the electrical field multiplied by conductivity and divided by mass density. Thus, the relation between SAR and power is linear, as it could be expected. In the same manner, the effect of the dielectric values of

human body on SAR is frequency dependent.

4.3 Testing an Antenna on Simulated and Real Human Arm

Body tissues are extremely lossy and have a high dielectric constant and electrical conductivity, which results in a large loss in the RF signal strength transmission from the body to free space. Therefore, as the human body absorbs a large amount of radiated electromagnetic power, it is normal for the antenna characterizations to significantly decrease.

The electromagnetic coupling between the antenna and the lossy human body tissue affects the antenna performance, including the matching, resonance frequency, efficiency, and gain [47]. This leads to a shift in the resonance frequency of the antennas. Based on the available information, our developed model can provide a closer approximation of the performance of the antenna than the homogenous model does. Because the model is made up of multiple layers with varying permittivity, it is similar to a voxel model to some extent.

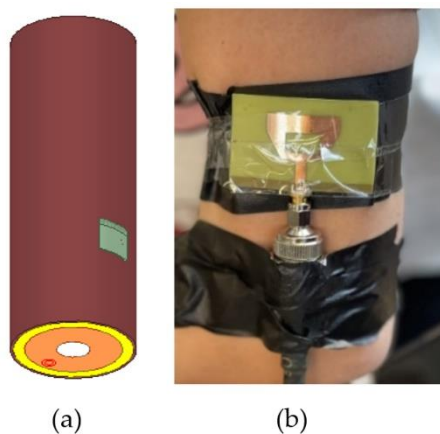


Figure 4.5: The microstrip patch antenna on the simulated human arm model of (a) 45 mm radius versus (b) the fabricated microstrip patch antenna on real human arm subject of the same radius.

Thus, the resonance frequency will shift to a higher band. When the antenna is bent around the simulated human arm model of radius 45 mm, the resonant frequency is shifted to 2.6 GHz with S_{11} at about -20 dB. This is the same case as shown in Figure 4.5, when the fabricated patch was placed on a real human arm subject with the same radius of 45mm. The measured reflection coefficient is decreased due to effects of impedance mismatching of the lossy human tissue that provides the dielectric loading.

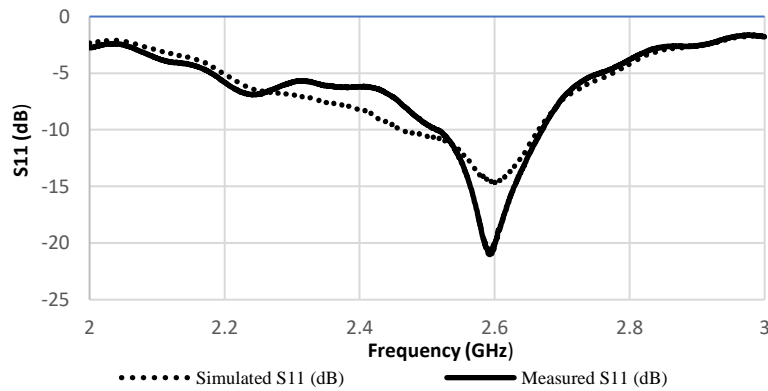


Figure 4.6: Simulated return loss with the presence of the simulated human arm model versus measured return loss on a real human arm of the same radius 45 mm as simulated.

However, the measured results show some degradation in the performance of the antenna. Thus, for better results, future research should add a layer with relative permittivity equal to the average permittivity of the arm tissue (skin, muscle and bone) and thickened equal to the average diameter of the human arm. In this case, the general results will be improved.

Thus, considering the dielectric properties of human tissues, there is an acceptable penetration ratio of the antenna into the body, which is verified by the good impedance matching obtained from the simulation and measurement procedures as shown in Figure 4.6.

According to [42], antenna bending will induce a shift in resonant frequency.

Moreover, additional shift will occur in the presence of a human body. Furthermore, though the resonance was obtained at 2.6 GHz (Figure 4.5) near the arm with maximum bending and the design was optimized at narrow band 2.4 GHz in free space without bending, the study relies on obtaining the scattering parameters S21 of the two antenna pairs over [2,3] GHz. The dielectric properties of the human arm phantom were updated each time the frequency of the antenna is varied over [2,3] GHz because they are frequency dependent [46].

However, the measured results show some degradation in the performance of the antenna. Thus, for better results and as a future work, adding a layer with relative permittivity equal to the average permittivity of the arm tissue (skin, muscle and bone) and thickened equal to the average diameter of the human arm. In this case, the general results and accuracy will be improved.

4.4 Transmit/Receive Antennas on a Simulated Heterogenous Human Arm phantom and a Real Human Arm

The high-water content of our bodies provides a low-loss channel for signal propagation. The transmitted signal flows through the low-resistance layers of the body below the skin and is picked up by the antenna on the receiver side. In this work, the signal is capacitively coupled to the skin layers of the human body, which then flows through the conductive layers below the skin and is finally picked up capacitively at the other on-body antenna receiver.

To analyze the possible performance of antennas on a human arm, the transmitting antenna is attached to one side of the upper human arm and the receiving antenna is attached to the opposite side as shown in Figure 4.6. The simulated human arm model was designed based on similar dimensions to the real human arm subject. This is done by

optimizing the different tissue thicknesses so that the transmission coefficient of both cases, simulated agreement. To determine the transmission coefficient scattering parameters of antennas, two microstrip patches were fabricated and placed 6.25 cm apart in free space as shown in Figure 4.7. The distance must be at least a half wavelength to avoid mutual coupling [40]. The data obtained, shown in Figure 4.7, indicates a high correlation of the scattering transmission coefficient waveforms between the simulated model and the real human arm.



Figure 4.7: The fabricated pair of antennas are placed on a real human arm of radius 45 mm to examine the transmission coefficient.

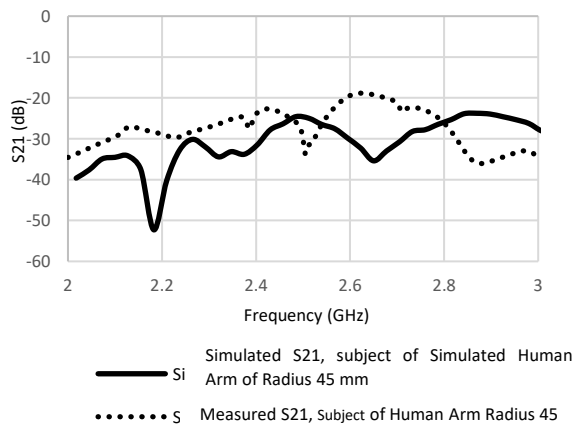


Figure 4.8: show the measured versus the simulated transmission coefficient S_{21} response of a pairs of antennas in free space and on simulated human arm modeled close to the real

human arm subject of radius 45mm respectively.

In this setting, the patch functions by emitting continuous RF waves and the receiving patch captures these waves. The properties of the reflected waves and the transmitted waves, in terms of scattering parameters or S parameters, were used and analyzed to determine the variation in blood pressure.

CHAPTER 5

ARTERIAL BLOOD PRESSURE ESTIMATION USING TRANSMISSION COEFFICIENT AND DATA ANALYSIS BY MEANS OF ASSESSMENT OF BRACHIAL DIAMETER CHANGE

The dual-pair antenna module implemented here is used to measure pulse signals at two points along the human arm at close distances. In detail, this technology focuses on transmission coefficient data analysis combined with an arterial blood flow algorithm, which in turn, utilizes the relative change in brachial artery diameter to determine blood pressure. Analytic algorithms can detect the feature points of variation in blood pressure with respect to variation in brachial artery thickness and radius ratio.

The proposed method analyzes the EM radiation from a pair of metallic microstrip patch antennas. The latter are made of epoxy material. This innovative BP measurement antenna is compact, lightweight, unobstructive and has low power consumption of about 50 mW.

5.1 The Proposed Blood Pressure Determination Method

There is no exact and direct relation between EM wave propagation and pressure. Meanwhile, the developed relationship between transmitting and receiving antennas depends on the change of reflected EM waves out of the antennas and related to the change in artery radius and thickness. This means any change in the properties of (h/R) ratio of the artery can be determined by the change in the shape of electromagnetic radiation waves between the pair of antennas and can be indirectly related to variations in blood pressure levels [48-50]. Considering that a larger brachial artery radius is

associated with a greater risk of elevated levels of blood pressure [50-52], the new proposed topology is shown in Figure 5.1 and is based on two critical factors to detect the variations in blood pressure: (i) the change in the brachial artery (BA) thickness-to- radius specifications, and (ii) the change in dielectric constant.

Commonly blood is a good conductor of electricity [48], therefore modeling the electromagnetic changes associated with blood flow plays a significant role in assessing hypertension.

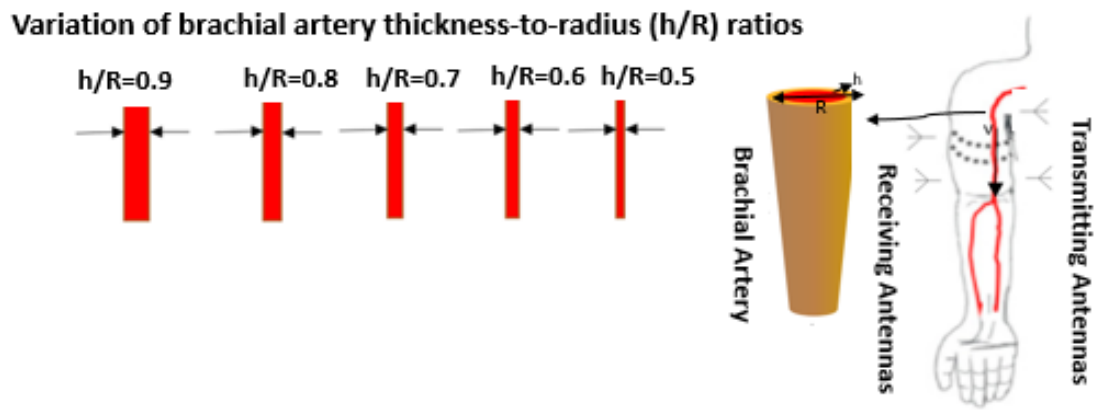


Figure 5.1. Illustration of proposed method related to brachial artery h/R ratio variation in respect to blood pressure estimation. Healthy elastic arteries=Normal BP and elastic artery stiffening= increase CV risk. The arterial vessel is often modeled as an elastic cylindrical tube. The simulation would be performed at five instances of brachial artery diameters to mimic the condition of blood flow. Although the above simulation model lacks blood flow, the consideration of different arterial diameters partly compensates for the hemodynamic effects. The choice of different arterial diameters complies with the characteristics of the arterial system. It was reasonably assuming that the brachial artery diameter changes uniformly at each dielectric characteristic change of the flow of blood, fat, muscle, bone and skin

Blood flow modeling was performed by considering the main artery of the upper arm and the brachial artery (BA) modeled as an elastic tube. The assessment of arterial wall (h/R) ratio or brachial hardening has a prognostic role in the prediction of hypertension and the brachial artery is a good reflector of central blood pressure [48-52].

Its diameter varies periodically with the heartbeat. The EM waves emitted from the EM microstrip patch antennas, are transmitted through the human arm model and are affected by the different conductivity and permittivity tissue layers ranging from 2 GHz to 3 GHz. The latter goes deeper into the skin, fat, muscle, bones, veins and arteries where, these radiations are tested carefully and are proven to be safe and effective on the human body without any harmful effects. In short, the variations are transmitted and reflected in the form of waves, leading to an effective relationship between the transmission coefficient, pulse wave velocity and the change in arterial diameter.

5.2 Why is Thickening of Artery Wall Important?

Previous studies found that arterial wall thickening, or hardening has a prognostic role in the prediction of high blood pressure levels [50]. This study standardizes the method for the assessment of brachial thickness and radius and determines whether this brachial ratio can be used as a surrogate marker of future elevated levels of blood pressure.

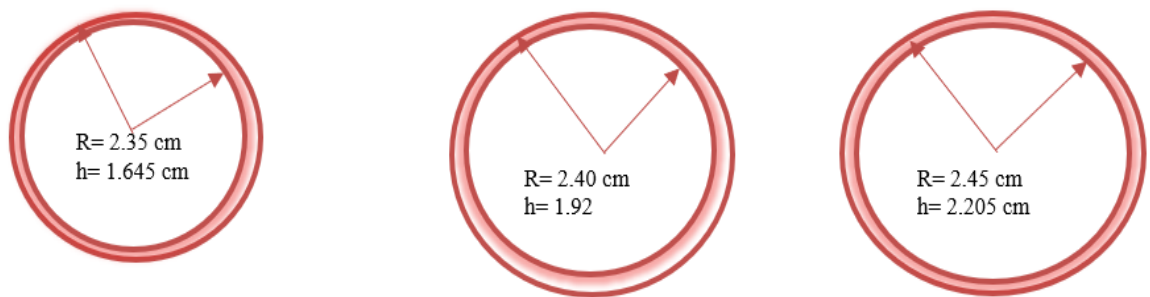


Figure 5.2: Brachial artery various thickness/radius ratio associated to blood pressure variations.

According to the study conducted, the simulated HFSS results validate that early minimum diameter lies between 4.3 mm and 4.5 mm, while the maximal brachial artery

diameter varies between 4.6 mm and 4.90 mm and is referred to hypertensive people. It is proved in medical studies that the prevalence of cardiovascular risk factors increases with the increase in brachial artery diameter.

The new indirect approach depends on the application of a transmission coefficient between the two pairs of microstrip antennas to model the arterial diameter variations so that useful blood pressure parameters can be easily derived.

5.3 Method I: Direct Pulse Transit Time Method by Means of Assessment of Brachial Artery Diameter Change and Pulse Wave Velocity.

Our main goal is to monitor BP changes through a continuous, noninvasive, and most importantly, cuffless technique. For this purpose, the pulse transit time (PTT) method has received much attention over recent decades because of its capability to evaluate pulse wave velocity (PWV) and hence track BP change as illustrated in Figure 5.3.

Pulse transit time (PTT) is defined as the estimated time delay of the pulse signal between two sites along the artery. Usually, the arterial pulse wave can be measured by blood volume changes in the arteries using non-invasive sensors placed at the measurement sites as shown in Figure 5.3.

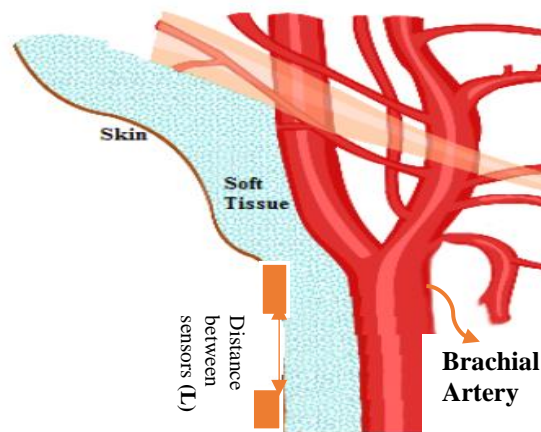


Figure 5.3: Placement of patch antennas over brachial artery to detect blood pulse waveforms.

Two separate pulse recordings over a known distance were obtained. Hence, the distance (L) between the two sensors allows calculation of PWV as indicated in equation 2.1. The innovative method is illustrated by:

1. Three primary simulations of brachial artery h/R fluctuation for the same human arm model, which demonstrate the transmission coefficient waveforms between the two pairs of antennas.
2. The time shift delay between the two waveforms of both sensors is used to estimate PTT at different artery thicknesses and radius coefficients. The smaller PTT values result in BP estimation with less sensitivity and thus less accurate BP monitoring.
3. PWV can be calculated based on the Bramwell–Hill formula and is therefore indirectly related to arterial distensibility.
4. Arterial distensibility is related to mean arterial pressure through regression analysis that reflects trends in blood pressure over the longer term as well as

indicates abrupt changes in arterial systolic and diastolic blood pressures as shown in Figure 5.8.

5.3.1 Measuring Transmission Coefficient (S_{21}) in Three Different Cases:

PTT has been estimated from the differences of the maximum slope points between two signals as shown in Figure 5.4. This method permits non-invasive, continuous and cuffless BP monitoring. The proposed method uses two separate pulse recordings over a known distance. The distance between the two measured placements is reduced to increase convenience. It is set to half wavelength of 6.25 cm at 2.4 GHz operating frequency. Placing both sensors at the central part of the brachial artery, a communal problem of measuring peripheral BP values is avoided. The changes in artery blood volume characteristics are modeled as changes in blood artery diameters.

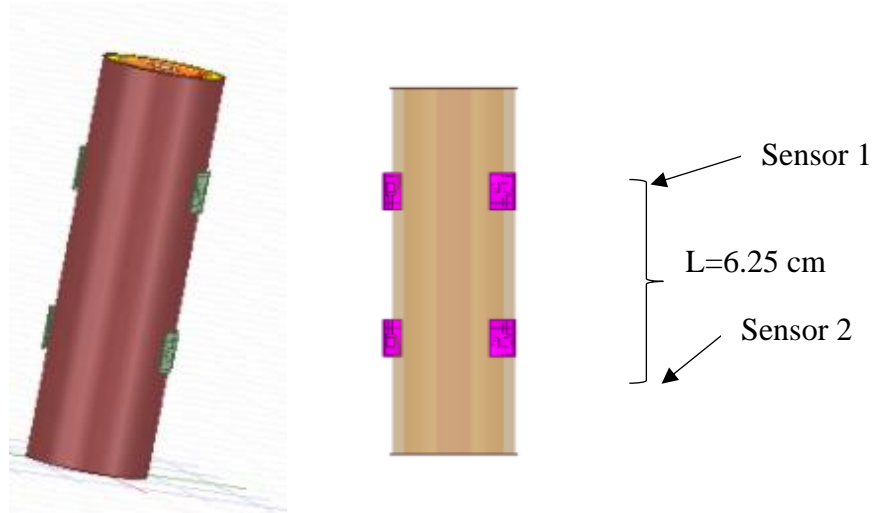
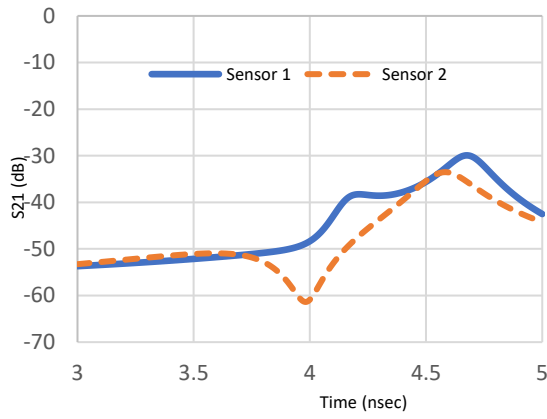


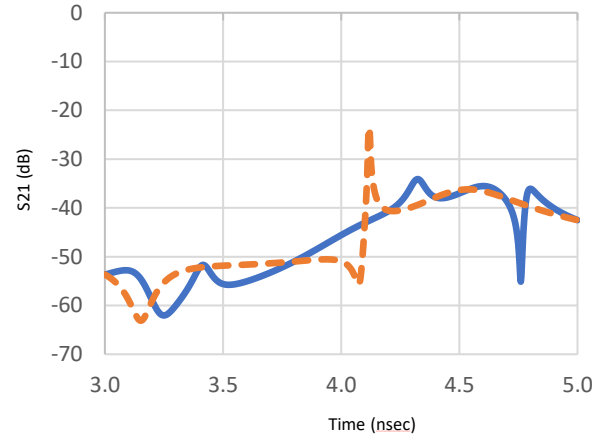
Figure 5.4: A pair of transmitting/receiving antennas bent over cylindrical multi-layer human arm model developed in ANSYS HFSS. EM waves out of the antennas can reach the targeted brachial artery along with the wide dielectric characterization range. L = length from the first sensor to the second; PTT = time taken for the pulse wave to propagate from the upper side (1) to lower side of the brachial artery (2). Based on the methodology of this study, the PWV-PPT relationship was noted for three distinct cases reflecting the effect of blood flow and thus blood pressure estimation. The cases were investigated with different artery h/R ratios of 0.5, 0.7 and 0.9.

5.3.2 Computing PWV with PTT

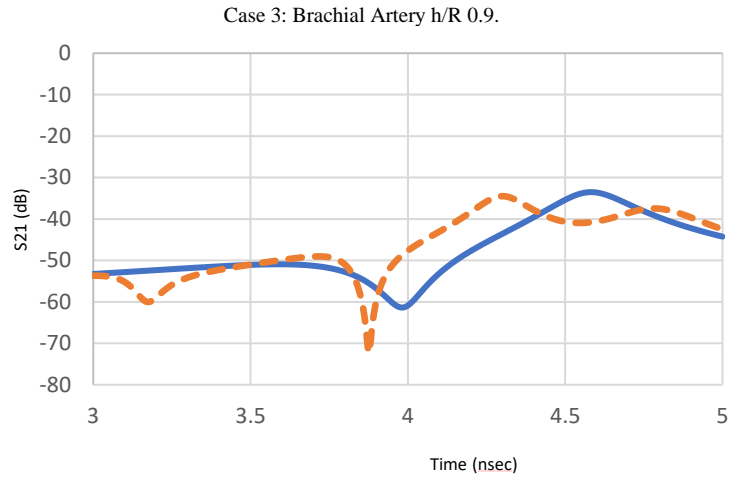
After PTT estimates were extracted as the time difference between proximal and distal transmission waveforms between the two pair of sensors presented previously in Figure 5.5, the Bramwell-Hill formula was applied to compute the PWV from the distance and pulse transit time (PTT). The PWV-PTT relationship is noted in the three different brachial artery h/R ratios change. The arterial thickness to radius varies with the blood vessel volume variation and thus arterial BP. The accuracy of BP estimation is affected if the arterial diameter is ignored.



Case 1: Brachial Artery $h/R = 0.5$.

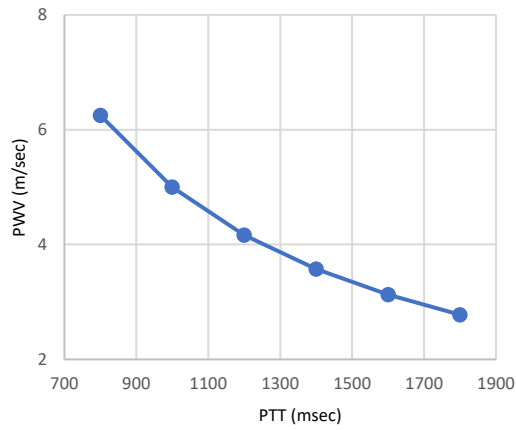


Case 2: Brachial Artery $h/R = 0.7$.

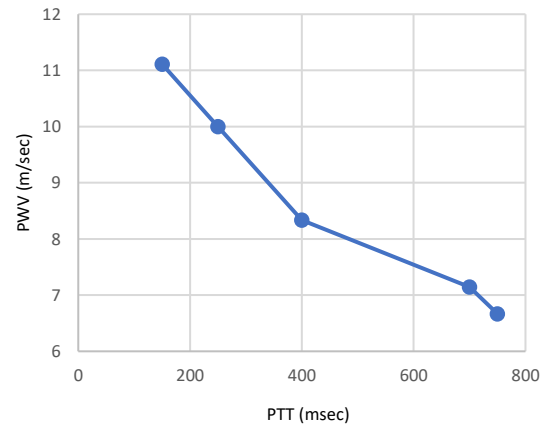


Case 3: Brachial Artery $h/R = 0.9$.

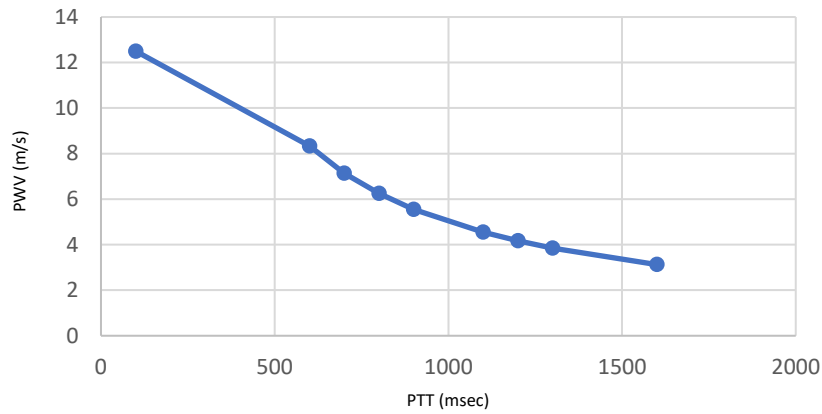
Figure 5.5: Three Cases of simulation results of transmission coefficient variation in the time domain for the human brachial artery of h/R ratios =0.5, 0.7 and 0.9 in time domain analysis. PTT is inversely related to BP through PWV calculation of first sensor and second sensor.



Case 1: Brachial Artery Thickness to Radius 0.5.



Case 2: Brachial Artery Thickness to Radius 0.7.

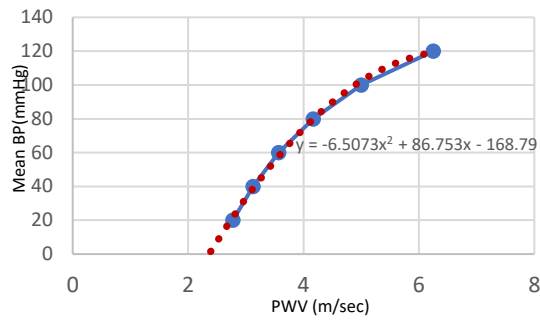


Case 3: Brachial Artery Thickness to Radius 0.9.

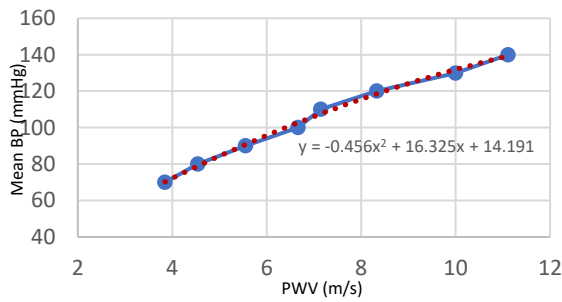
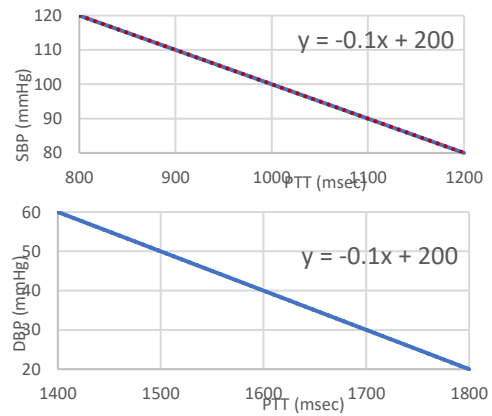
Figure 5.6: Simulation results of PTT- based pulse measurement dual sensors: Through this variation, PTT estimates for human artery of thickness/radius ratio $h/R=0.5$, 0.7 and 0.9 . PTT are extracted and then PWV can be calculated to provide a comprehensive overview of the blood pressure variation level.

5.3.3 Regression Equations to Find BP

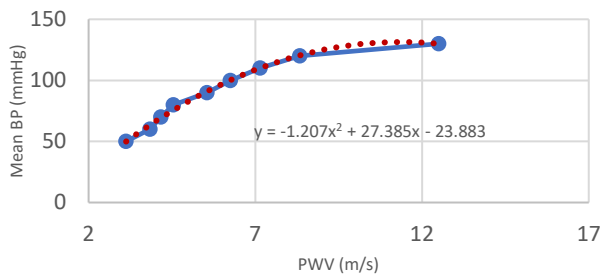
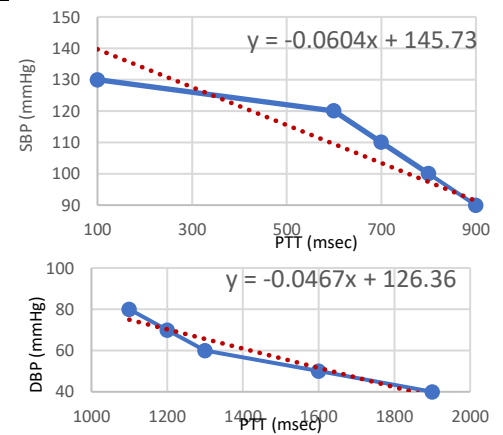
Whilst the PWV and PTT levels were set at normal values. The regression routine is shown in Figure 5.7 as a red dotted line. The correlation between the and diastolic blood pressure conditions. However, as the varying brachial artery coefficients increase, there will be an increase in blood pressure levels [50].



Case 1: Brachial Artery h/R of 0.5.



Case 2: Brachial Artery h/R of 0.7.



Case 3: Brachial Artery h/R of 0.9.

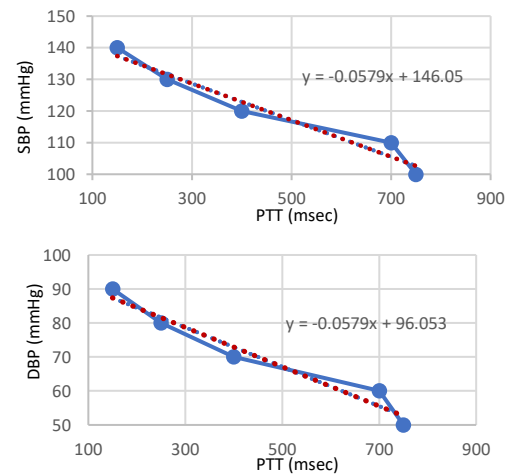


Figure 5.7: Mean BP versus PWV for the brachial artery of h/R ratios of 0.5, 0.7 and 0.9, with linear regression trend line. In addition, the relationship of PTT to Systolic BP with a straight line representing linear regression and the relationship of PTT to Diastolic BP with a straight line representing linear regression.

5.2.4 Summary

To our knowledge, the relationship between electromagnetic waves, PTT, and arterial pressure has not been previously systematically studied. This is an innovative step that relates the PTT, PWV, and BP in detail through simulations based on varying the arterial specifications. It is to be noted that this method requires no calibration. As the arterial pressure changes increased, the PTT decreased significantly. The maximal PWV of 11 m/s corresponds to high systolic and diastolic blood pressure levels. Non-linear curve fitting (Figure 5.7) using MATLAB to estimate the systolic and diastolic blood pressures of the collected data based on variation of age and obesity. Table 5.1 shows a comparison summary of the estimated PTT, PWV, and arterial BP of different arterial h/R ratios. The highest brachial artery h/R ratio presents the highest PWV and, consequently, the highest levels of blood pressure.

Table 5.1: Summary of estimated PTT, PWV and mean BP in the three studied cases.

Parameters	Case 1:h/R=0.5	Case 2: h/R=0.7	Case 3: h/R=0.9
PTT (s)	0.8- 1.8	0.15-0.75	0.1-1.6
PWV (m/sec)	2.7-6.2	6.5-11	3-13
Mean BP	60-120	50-110	50-140
Systolic BP	80-120	100-140	100-140
Diastolic BP	20-60	40-80	90-130

PTT: Pulse Transit Time
PWV: Pulse Wave Velocity
h/R: thickness-to-radius

5.4 Method II: Mathematical Approach Towards Pulse Wave Velocity Determination

The Moens-Korteweg (MK) given in equation 2.2, is used to prove the previously proposed innovative model. The general aspect of this analytical method is reliable for

continuous, cuffless, and noninvasive blood pressure monitoring techniques. The pressure pulse propagation speed passing along the artery, is a function of its elasticity and pressure with the underlying condition that brachial artery geometries are dynamic. The condition is based on the variation of the h/R ratio for a healthy person (0.08 to ~ 0.22) before artery deformation and increases significantly after deformation to reach 0.5 to ~ 0.9 for a person with an arterial disease [48-54]. The artery deformation is due to variations in blood pressure levels. Another important application of the MK equation is to determine the arterial strain “ E_{inc} ” because of its application in the prediction of elevated blood pressure levels. E_{inc} is also an intrinsic measure of arterial wall stiffness [55, 56]. The connection will be shown to be due to the elasticity of the artery walls because any increase in pressure will lead to an increase in the artery cross-section [57]. Thus, there is a positive correlation between the brachial artery elastic properties, the thickness and the artery radius, the arterial strain (E), and the PWV as specified in equation 2.2 and equation 2.3.

5.4.1 Correlation Between Stiffness and PWV

In this thesis, no assumptions are made to establish a relationship between the PWV and BP. The arterial cross-sectional area has been shown to be a reliable marker of BP.

First, the brachial artery blood properties have been modeled, for which simulation has been performed using three different thickness to radius thickness variations. Second, the findings of this research investigate the arterial wall thickness either for a healthy person or one with arterial disease. Thus, the purpose of this study is to determine the positive correlation between brachial artery elastic properties such as the

thickness, the artery diameter, and the arterial strain (E), PWV and consequently the prediction of any cardiovascular risk factors.

The arterial stiffness considered here fits the human blood pressure range (5 kPa to ~ 20 kPa), in which $E_0 = 563 \text{ kPa}$ at zero blood pressure and ζ is used to describe the brachial artery material property.

Our proposed method shows the increase in PWV is identified by the increase in the wall stiffness as shown in Figure 5.9. Figure 5.9 shown below presents a summary of PWV and E estimates from brachial artery thickness/ratio variation before any deformation. In general, the artery thickness is not constant for the human artery; the

Table 5.2: Summary of PWV and E estimates for different values of h/R ratios before artery deformation.

	Pulse Wave Velocity for different values of different h/R ratios							
$E(\text{kPa})$	$h/R=0.08$	$h/R=0.1$	$h/R=0.12$	$h/R=0.14$	$h/R=0.16$	$h/R=0.18$	$h/R=0.2$	$h/R=0.22$
25	0.971	1.086	1.190	1.285	1.374	1.457	1.536	1.611
50	1.374	1.536	1.682	1.817	1.943	2.117	2.172	2.278
75	1.682	1.881	2.060	2.225	2.379	2.523	2.660	2.790
100	1.943	2.172	2.379	2.570	2.747	2.914	3.071	3.221
125	2.172	2.428	2.660	2.873	3.071	3.258	3.434	3.602
150	2.379	2.660	2.914	3.147	3.365	3.569	3.762	3.945
175	2.570	2.873	3.147	3.400	3.634	3.855	4.063	4.261
200	2.747	3.071	3.365	3.634	3.885	4.121	4.344	4.556
225	2.914	3.258	3.569	3.855	4.121	4.371	4.607	4.832
250	3.071	3.434	3.762	4.063	4.344	4.607	4.856	5.092

thickness-to-radius ratio has an average of h_0/R_0 0.08 to ~ 0.22 before deformation.

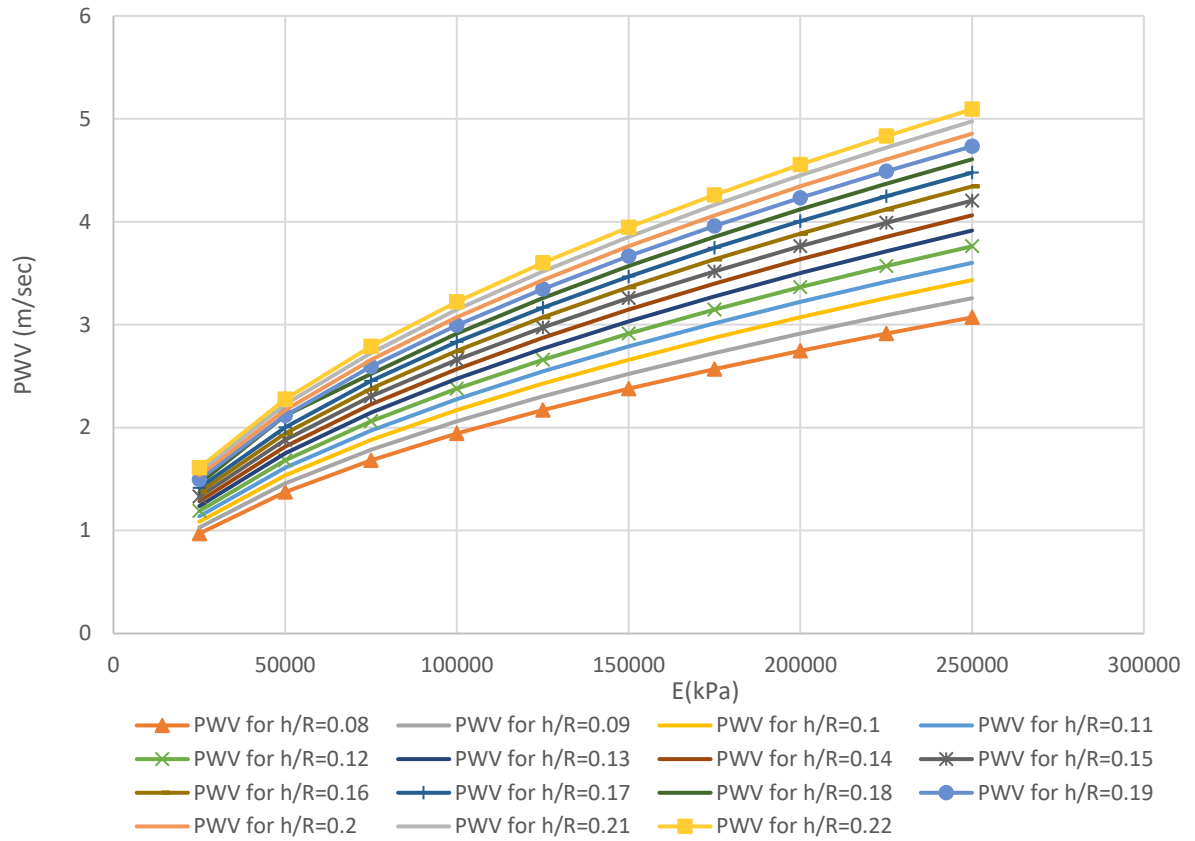


Figure 5.8: The theoretical, i.e., Moens-Korteweg, relationship between the PWV versus artery stiffness (equivalent modulus) E (based on the parameters used in the simulation) for a human brachial artery before deformation due to the blood pressure.

Changes in arterial stiffness can be used to facilitate the relationship between the brachial thickness to radius ratio and pulse wave velocity. Table 5.2 presents a summary of PWV and E estimates for different values of the thickness/radius ratio (h/R) after deformation due to blood pressure. This proves that the large arteries gradually lose their elasticity and become stiffer which leads to an increase in blood pressure levels.

Table 5.3: Summary of PWV and E estimates for different values of Thickness/Radius ratio (h/R) after deformation due to blood pressure.

E	h/R	PWV for h/R=0.5	PWV for h/R=0.6	PWV for h/R=0.7	PWV for h/R=0.8	PWV for h/R=0.9
25000	0.5	2.428	2.660	2.873	3.071	3.258
50000	0.6	3.434	3.762	4.063	4.344	4.607
75000	0.7	4.206	4.607	4.976	5.320	5.643
100000	0.8	4.856	5.320	5.746	6.143	6.516
125000	0.9	5.430	5.948	6.424	6.868	7.285
150000		5.948	6.516	7.038	7.524	7.980
175000		6.424	7.038	7.602	8.126	8.619
200000		6.868	7.524	8.126	8.687	9.214
225000		7.285	7.980	8.619	9.214	9.773
250000		7.679	8.412	9.086	9.713	10.302

As shown in Figure 5.10, these findings suggest a cause–effect relationship between the thickness/radius brachial artery and the increase in pulse wave velocity. *Thus*, establishing it as a reliable prognostic marker for detecting elevated levels of blood pressure.

Taking into account the link between the arterial stiffness changes, in response to variation in blood pressure levels. This concludes that as the aorta stiffens, the velocity of the pressure wave increases, causing augmentation of the systolic blood pressure (SBP) and of the diastolic blood pressure (DBP).

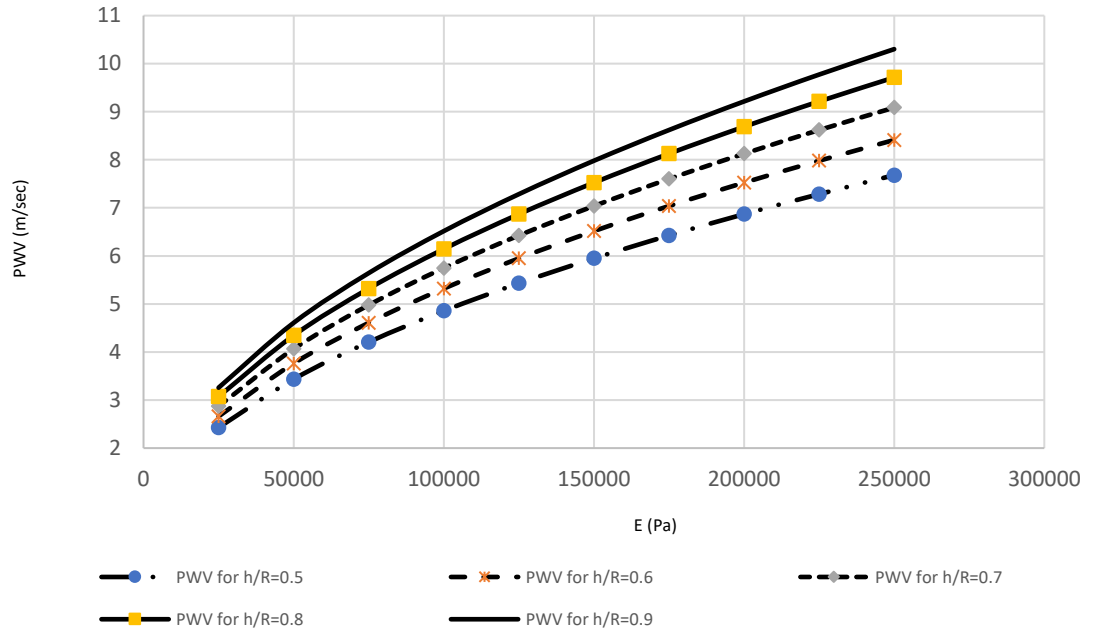


Figure 5.9: The theoretical, i.e., Moens-Korteweg, relationship between the PWV versus artery stiffness (equivalent modulus) E for a human brachial artery after deformation due to blood pressure.

By observing the increase of PWV in terms of increase of arterial wall thickness, a simple analytical study is noted. Using the mathematical “**least square approach**” analysis to determine the relation between BP and PWV can be represented by the quadratic equation:

$$BP = a * PWV^2 + b \quad (5.9)$$

where a and b are scaling coefficients that depend on the material properties and geometry of the artery. This formula, derived from the PWV-arterial stiffness relationship curve, can be used to determine the blood pressure in continuous, cuffless, and noninvasive blood pressure monitoring. Figure 5.10 defines a linear relationship between

the increase in PWV and the change in blood pressure (kPa). A pressure measured in kilopascals can be converted to a millimetre of mercury reading using the following conversion factor: A kilopascal is equal to 1000 pascals, which corresponds to one mmHg, which in turn, equals to 133.322 pascals.

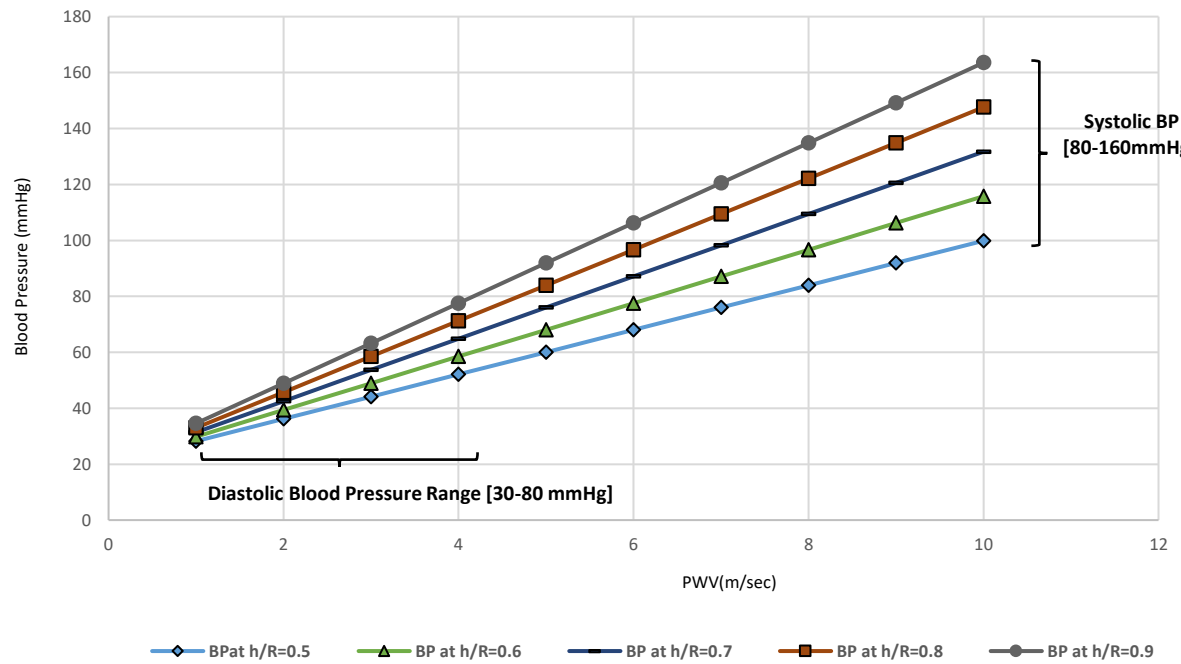


Figure 5.10: Blood pressure P versus normalized PWV for human brachial artery. Effects of wall thickness divided by vessel radius in arterioles (after deformation) on blood pressure (in mmHg). At any level of mean arterial pressure, the absolute risk of a composite cardiovascular outcome increased in relation to aortic PWV.

As shown in Figure 5.11 the blood pressure BP increases, the artery stiffens (i.e., increases the tangent modulus E based on Equation 2.2), leading to an increase in PWV. The higher the PWV is associated with higher risk for a cardiovascular event.

Figures 5.11 and 5.12 depicts the dependence of PWV on pressure for the Systole

Phase (marked as “SBP”) and the Diastole Phase (marked as “DBP”) for the vessel of different thicknesses of a human aorta. Thus, the mathematical approach shows that any change in BP is directly proportional to the change in arterial cross-sectional area.

Equation 5.9 can be divided into a system of two equations: the DBP and SBP equations. So, BP_{Dia} and BP_{Sys} can be estimated according to the blood flow information by derived linear equations as:

$$BP_{Sys} = a_1 \times PWV + b_1 \quad (5.10)$$

$$BP_{Dia} = a_2 \times PWV + b_2 \quad (5.11)$$

where the a_1 and a_2 are weighting factors of PWV, and the linear basis variables, b_1 and b_2 , are statically calculated by the population in the experiment. The weighting factor $a_1 = 0.84$ and $a_2 = 0.66$, and the basis variables, $b_1 = 6.39$ and $b_2 = 5.29$, were applied in this study.

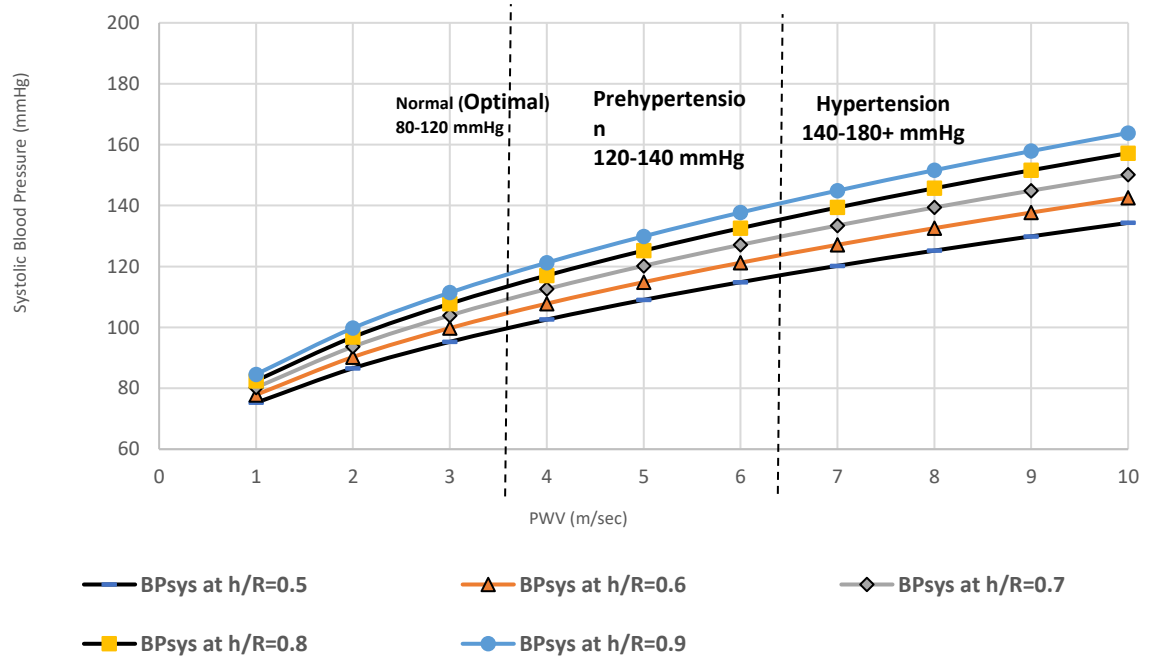


Figure 5.11: Relationship between pulse-wave velocity and systolic blood pressure (in

mmHg).

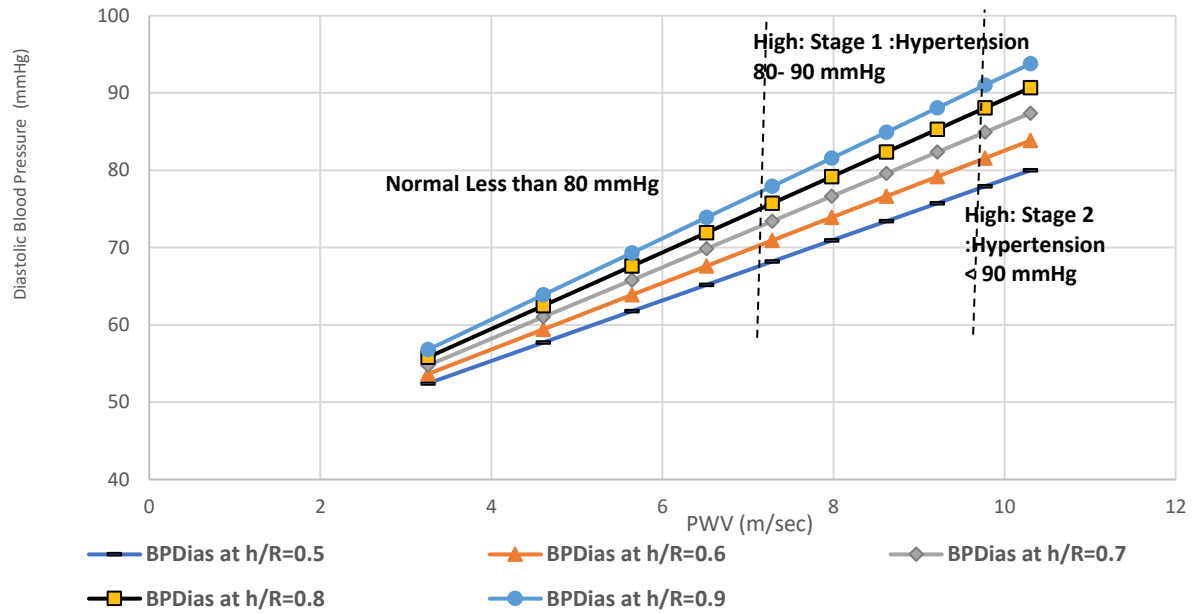


Figure 5.12: Relationship between pulse-wave velocity and diastolic blood pressure (in mmHg).

It is well shown that the nearly linear increase in the wall thickness to vessel radius ratio (h/R) results in increasing systolic and diastolic pressure. Predicted effects of driving pressure on the ratio of wall thickness to vessel diameter are consistent with the simulated experiment of two facing antennas on a human arm. Both the proposed PTT-BP and the mathematical models were successful at representing any hypertension.

5.5 Summary

Table 5.4 shows the summary of the two methods. There is a good consistency between the results of the two methods. According to the results, by comparing the PWV, SBP and DBP values, both models show good agreement and high accuracy in a systematic and detailed algorithm.

Table 5.4: Summary table comparing the two proposed methods for blood pressure estimation.

Parameters	Case 1: h/R=0.5		Case 2: h/R=0.7		Case 3: h/R=0.9	
	Transmission	Moens	Transmission	Moens	Transmission	Moens
	Coefficient-PTT method	Korteweg equation	Coefficient-PTT method	Korteweg equations	Coefficient-PTT method	Korteweg equation
PTT (s)	0.8-1.8	-	0.6-1.6	-	0.1-1.3	-
PWV (m/sec)	2.7-6.2	2. 5-7.5	6.5-11	3- 9	3-13	3.5- 10.5
Mean BP	60-120	3 0-100	50-110	30 -130	70-140	40- 160
SBP	80-120	8 0-130	100-140	80 -150	100-140	90- 165
DBP	20-60	5 5-80	50-90	55 -85	50-90	55-95

CHAPTER 6

CONCLUSION

There is no previously published information regarding the estimation of BP from the output of two microstrip patch antennas placed on a human arm. This paper proposes a technology using a flexible and wearable microstrip patch antenna that analyzes the EM radiations out of a pair of metallic patch antennas of epoxy substrates to track patient BP continuously. This innovative BP measurement device is compact, lightweight, unobstructed, and with low power consumption at about 50 mW for each metallic sensor.

We outline the use of a microstrip patch antenna on a simulated human arm and also test the antenna on a human arm subject. The result shows that the performance of the proposed antenna is dependent on the extent of antenna bending but still operates efficiently within the expected curvature of the human arm for measures of brachial artery BP. The findings further highlight the importance of taking into account accurate dielectric properties of the constituent tissues in the estimation of EM medical technologies. The specific absorption rate was also analyzed and confirmed to have no adverse biological health effects on tissues.

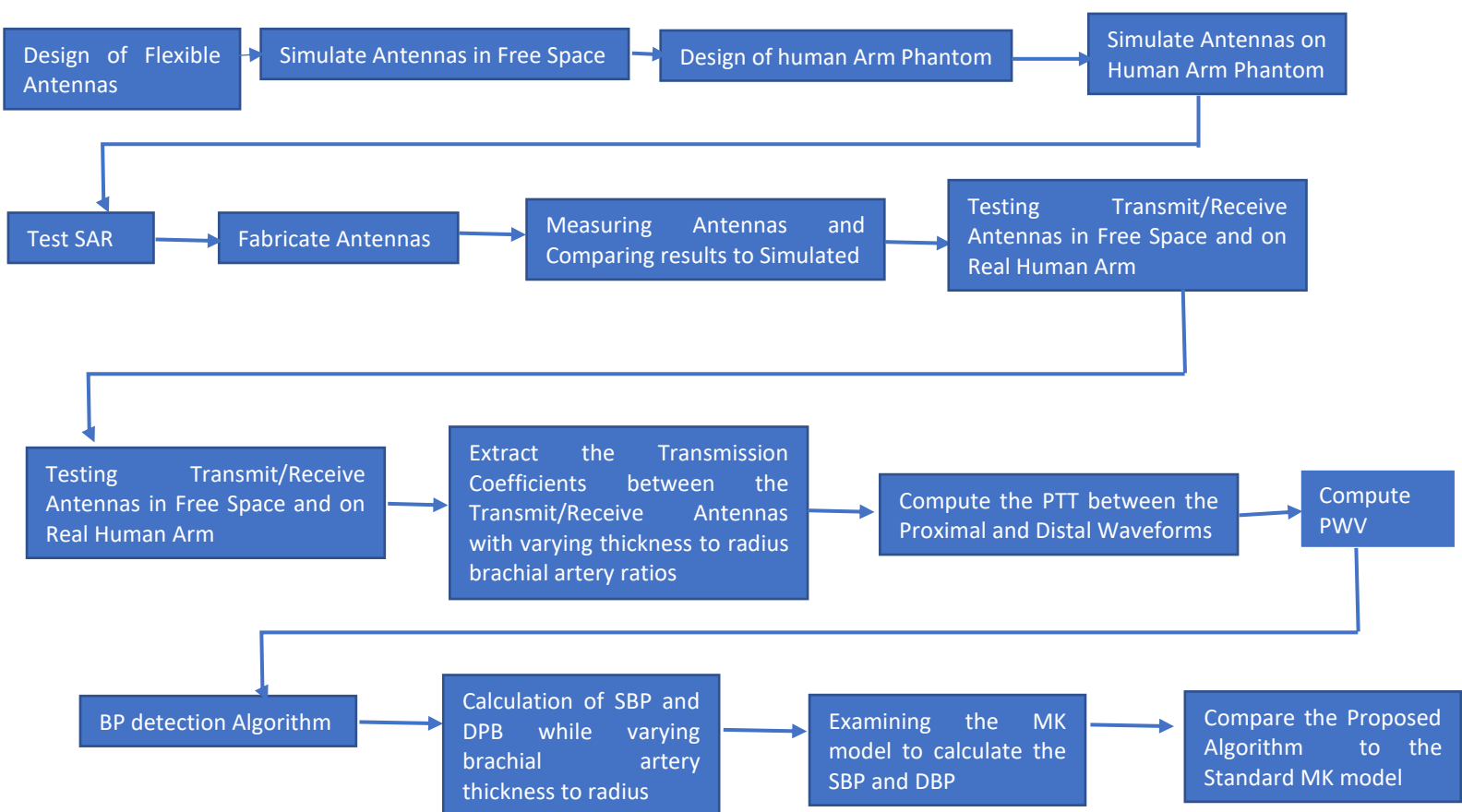
In detail, the non-invasive high-frequency patch microstrip technology focuses on the emission of electromagnetic waves into the tissues to provide accurate simulated changes in BP measurements. The new model first identifies the pulse transit time of a pulse wave. The latter is defined as the time difference between the variation of the distal and proximal transmission coefficient waveforms between two pairs of sensors with respect to varying artery coefficients. The distance between the two pairs of antennas is

equally set at half the wavelength. Second, PWV can be computed from pulse transit time (PTT) via $PWV = L/PTT$, where L is the distance between the two points of propagation. The correlation between local PWV and BP measures is also explored. The artery size variation was dependent on the artery before and after deformation to prove the presence of blood pressure due to the thickening and hardening of the artery. Finally, algorithms and regression models are discussed, so that PWV is related to SBP and DBP.

To verify the results of the proposed simulation model, a mathematical model was suggested to describe the vessel radius to thickness ratios under different medical conditions. The model was based on the standard MK equation along with the Hughes equation, but with consideration that the artery geometry is dynamic rather than static. The MK equation models a relationship between brachial artery size variation and pulse wave velocity. The latter can be easily computed while assessing the arterial stiffness in the range of blood pressure. The use of the MK model shows excellent consistency with the proposed model, so that PWV can be computed to assess the arterial strain in the range of blood pressure.

When the developed model and the MK model do not hold any assumptions and take into consideration the thickness and radius of the artery change with any rise or drop in blood pressure levels, the pulse pressure propagation speed along with the artery stiffness also vary.

Thus, in this study, the PWV is directly related to arterial stiffness, an analytical model is established to yield a relationship between blood pressure and pulse wave velocity. The results of both methods successfully demonstrate how the radius estimates, PTT and PWV, along with EM antenna transmission propagation characteristics, can be used to estimate continuous BP non-invasively. The methodology is illustrated below.



A significant advantage of the proposed design is that it requires no calibration for accurate results after each usage and is inexpensive, comfortable, and highly accurate as it provides a desirable wearable option for home and office BP monitoring.

In summary, this simulated and real-time patient BP assessment provides the groundwork required to potentially develop a real-world non-invasive arterial pressure monitor system. The methodology of this system can be developed into a practical nano-wearable device that can provide timely and precise health-based care.

6.1 Advantages

The current antennas are small in size, flexible presenting low power, continuous and potentially wearable system. The highest improvement is obtained based on new algorithm to extract the *PTT* s which also has the advantage of simplicity. The system proposed is simple which requires no calibration compared to most of the traditional blood pressure measurement methods. In addition, compared to other pulse wave monitoring methods, such as PPG, the dual antenna system can provide central elastic brachial artery monitoring, removing the peripheral inaccuracies, which requires higher quality in the design of these sensors for recordings and processing in future work. This shows the potential of the microstrip antenna-based system to provide a simple wearable device, which can monitor *PTTs* and in results, beat-to-beat *SBPs*.

6.2 Limitations and Future Work

On the other hand, there are also some limitations to this new technique. First, on top of the antenna radiator, a layer of the flexible biocompatible epoxy must be added with a thickness of 0.03 mm. The addition of this layer is necessary to preserve the

antenna performance and to prevent direct contact between the radiator and the body tissues. Second, the system should be further validated through measurement on various arm sizes of healthy subjects and on subjects with different blood pressure levels and pathologies. Third, the relationship between PTT, the distance of the sensors, and the patch-to-skin pressure should be investigated. Fourth, the proposed structure should be compared against other structures to assess the advantages of each method. Fifth, the BP validation protocol should be expanded, and various BP perturbations should be applied to a larger study cohort.

Finally, for the prospective development, integration of all functions, including sensing, signal processing and wireless data transmission, into a dedicated system can be helpful to provide long-term and continuous blood pressure monitoring for personal healthcare.

REFERENCES

- [1] Roth, Gregory A., Catherine Johnson, Amanuel Abajobir, Foad Abd-Allah, Semaw Ferede Abera, Gebre Abyu, Muktar Ahmed et al. "Global, regional, and national burden of cardiovascular diseases for 10 causes, 1990 to 2015." *Journal of the American College of Cardiology* 70, no. 1 (2017): 1-25.
- [2] Goonasekera, C. D. A., and M. J. Dillon. "Measurement and interpretation of blood pressure." *Archives of disease in childhood* 82, no. 3 (2000): 261-265.
- [3] Muntner, Paul, Daichi Shimbo, Robert M. Carey, Jeanne B. Charleston, Trudy Gaillard, Sanjay Misra, Martin G. Myers et al. "Measurement of blood pressure in humans: a scientific statement from the American Heart Association." *Hypertension* 73, no. 5 (2019): e35-e66.
- [4] D. Herpin, T. Pickering, G. Stergiou, P. de Leeuw, and G. Germano, "Consensus Conference on Self-blood pressure measurement. Clinical applications and diagnosis," *Blood Press. Monit.*, vol. 5, no. 2, pp. 131-135, Apr 2000.
- [5] Ogedegbe, Gbenga, and Thomas Pickering. "Principles and techniques of blood pressure measurement." *Cardiology clinics* 28.4 (2010): 571-586.
- [6] Pickering, T.G.; Miller, N.H.; Ogedegbe, G.; Krakoff, L.R.; Artinian, N.T.; Goff, D. Call to action on use and reimbursement for home blood pressure monitoring: A joint scientific statement from the American Heart Association, American Society of Hypertension, and Preventive Cardiovascular Nurses Association. *Hypertension* 2008, 52, 10–29.
- [7] C. A. Balanis, *Antenna theory: analysis and design*. Hoboken, NJ: Wiley, 2016.
- [8] T.G. Pickering, D. Shimbo, and D. Haas, "Ambulatory blood-pressure monitoring," *N. Engl. J. Med.*, vol. 354, no. 22, pp. 2368-2374, June 2006.

- [9] H. Reims, E. Fossum, S.E. Kjeldsen, and S. Julius, "Home blood pressure monitoring. Current knowledge and directions for future research," *Blood Press.*, vol. 10, no.5-6, pp. 271-287, 2001.
- [10] Peter, L.; Noury, N.; Cerny, M. A review of methods for non-invasive and continuous blood pressure monitoring: Pulse transit time method is promising? *IRBM* 2014, 35, 271–282.
- [11] A. S. Meidert and B. Saugel, "Techniques for non-invasive monitoring of arterial blood pressure," *Frontiers in Medicine*, vol. 4, 2018.
- [12] Arakawa, Toshiya. "Recent research and developing trends of wearable sensors for detecting blood pressure." *Sensors* 18, no. 9 (2018): 2772.
- [13] Erdmier, Casey, Jason Hatcher, and Michael Lee. "Wearable device implications in the healthcare industry." *Journal of medical engineering & technology* 40, no. 4 (2016): 141-148.
- [14] Shuzo, M. Development of Wearable Sensor for Continuous Blood Pressure without Cuff Load. *Sci. Rep. Res. Inst. Eng. Kanagawa Univ.* 2012, 35, 2–7.
- [15] M. Pour Ebrahim, F. Heydari, T. Wu, K. Walker, K. Joe, J.-M. Redoute, and M. R. Yuce, "Blood pressure estimation Using On-body continuous wave radar and photoplethysmogram in various posture and Exercise Conditions," *Scientific Reports*, vol. 9, no. 1, pp.1-13 2019.
- [16] P. M. Nabeel, J. Jayaraj, and S. Mohanasankar, "Single-source PPG-based local pulse wave velocity measurement: a potential cuffless blood pressure estimation technique," *Physiological Measurement*, vol. 38, no. 12, pp. 2122–2140, 2017.

- [17] L. Peter, J. Kracik, M. Cerny, N. Noury, and S. Polzer, "Mathematical model based on the shape of pulse waves measured at a single spot for the non-invasive prediction of blood pressure," *Processes*, vol. 8, no. 4, pp. 442, 2020.
- [18] W.M. Nichols and M.F. O'Rourke, *McDonald's Blood Flow in Arteries Theoretical, experimental, and clinical principals*. 4th ed., Hodder Arnold Publication, London, 1998, ch. 3.
- [19] Huttunen, Janne MJ, Leo Kärkkäinen, and Harri Lindholm. "Pulse transit time estimation of aortic pulse wave velocity and blood pressure using machine learning and simulated training data." *PLoS computational biology* 15, no. 8 (2019): e1007259.
- [20] Bramwell, J. Crighton, and Archibald Vivian Hill. "The velocity of pulse wave in man." *Proceedings of the Royal Society of London. Series B, Containing Papers of a Biological Character* 93, no. 652 (1922): 298-306.
- [21] Baek, H.J.; Kim, K.K.; Kim, J.S.; Lee, B.; Park, K.S. Enhancing the estimation of blood pressure using pulse arrival time and two confounding factors. *Physiol. Meas.* 2010, 31, 145–157.
- [22] Kim, Eung Ju, Chang Gyu Park, J. S. Park, S. Y. Suh, Cheol Ung Choi, Jin Won Kim, S. H. Kim et al. "Relationship between blood pressure parameters and pulse wave velocity in normotensive and hypertensive subjects: invasive study." *Journal of human hypertension* 21, no. 2 (2007): 141-148.
- [23] Wang, Ting-Wei, and Shien-Fong Lin. "Wearable piezoelectric-based system for continuous beat-to-beat blood pressure measurement." *Sensors* 20, no. 3 (2020): 851.
- [24] N. Kathuria and B.-C. Seet, "24 GHz flexible antenna for Doppler radar-based Human Vital Signs Monitoring," *Sensors*, vol. 21, no. 11, p. 3737, 2021.

- [25] H. Zhao, X. Gu, H. Hong, Y. Li, X. Zhu, and C. Li, "Non-contact beat-to-beat blood pressure measurement using continuous wave Doppler radar," 2018 IEEE/MTT-S International Microwave Symposium - IMS, pp. 1413-1415 2018.
- [26] S. H. Woo, Y. Y. Choi, D. J. Kim, F. Bien, and J. J. Kim, "Tissue-informative mechanism for wearable non-invasive continuous blood pressure monitoring," Scientific Reports, vol. 4, no. 1, pp.1-6, 2014.
- [27] Lin, H., Lee, Y., Su, Y. and Chuang, B., 2011. Nanosecond Pulse Near-Field Sensing Based Non-Contact Physiological Signals Measurement. Advanced Materials Research, 301-303, pp.1214-1219.
- [28] Huynh, Toan Huu, Roozbeh Jafari, and Wan-Young Chung. "An accurate bioimpedance measurement system for blood pressure monitoring." Sensors 18, no. 7 (2018): 2095.
- [29] Ishizawa, Hidetoshi, Takashi Tanabe, Daiki Yoshida, S. Hamid R. Hosseini, Sunao Katsuki, and Hidenori Akiyama. "Focusing system of burst electromagnetic waves for medical applications." IEEE Transactions on Dielectrics and Electrical Insulation 20, no. 4 (2013): 1321-1326.
- [30] Hieda, Ichiro, and Ki Chang Nam. "Electric field measurement of the living human body for biomedical applications: Phase measurement of the electric field intensity." International Journal of Antennas and Propagation 2013 (2013).
- [31] Dorababu, N., Y. Ratna Kumar, K. Venkatesu, G. Karunakar, and G. S. N. Raju. "Electromagnetic energy in biological tissues." In 2008 10th International Conference on Electromagnetic Interference & Compatibility, pp. 385-390. IEEE, 2008.

- [32] Asghari, Ali, Amir Afshin Khaki, Asghar Rajabzadeh, and Arash Khaki. "A review on Electromagnetic fields (EMFs) and the reproductive system." *Electronic physician* 8, no. 7 (2016): 2655.
- [33] Ciombor, Deborah McK, and Roy K. Aaron. "The role of electrical stimulation in bone repair." *Foot and ankle clinics* 10, no. 4 (2005): 579-593.
- [34] Singh, Sarika, and Neeru Kapoor. "Health implications of electromagnetic fields, mechanisms of action, and research needs." *Advances in biology* 2014 (2014).
- [35] Federal Communications Commission. "Specific absorption rate (SAR) for cellular telephones." *Printed From Internet May 20* (2015): 2.
- [36] Murbach, Manuel, Esra Neufeld, Myles Capstick, Wolfgang Kainz, David O. Brunner, Theodoros Samaras, Klaas P. Pruessmann, and Niels Kuster. "Thermal tissue damage model analyzed for different whole-body SAR and scan durations for standard MR body coils." *Magnetic resonance in medicine* 71, no. 1 (2014): 421-431.
- [37] Xu LS, Meng MQ, Li BP. Effects of dielectric values of human body on Specific Absorption Rate (SAR) following 800 MHz radio frequency exposure to ingestible wireless device. *Annu Int Conf IEEE Eng Med Biol Soc.* 2009; 2009:5060-3. doi: 10.1109/IEMBS.2009.5334263. PMID: 19964854.
- [38] Kurian, Jobin, Upama Rajan, and Shinoj K. Sukumaran. "Flexible microstrip patch antenna using rubber substrate for WBAN applications." In *2014 International Conference on Contemporary Computing and Informatics (IC3I)*, pp. 983-986. IEEE, 2014.
- [39] Mohamadzade, Bahare, Raheel M. Hashmi, Roy BVB Simorangkir, Reza Gharaei, Sabih Ur Rehman, and Qammer H. Abbasi. "Recent advances in fabrication methods for flexible antennas in wearable devices: State of the art." *Sensors* 19, no.

- 10 (2019): 2312.
- [40] H. R. Khaleel, H. M. Al-Rizzo, D. G. Rucker, and T. A. Elwi, "Wearable Yagi microstrip antenna for telemedicine applications," in 2010 IEEE Radio and Wireless Symposium (RWS), 10-14 Jan. 2010, pp. 280-283, doi: 10.1109/RWS.2010.5434177.
- [41] M. E. Abbasi and K. Kabalan, "Revolutionizing the development of Wearable Antennas," 2019 International Workshop on Antenna Technology (iWAT), pp. 54-57, 2019.
- [42] S. M. Shah, N. F. A. Kadir, Z. Z. Abidin, F. C. Seman, S. A. Hamzah, and N. Katiran, "A 2.45 GHz semi-flexible wearable antenna for industrial, scientific and medical band applications," *Indonesian Journal of Electrical Engineering and Computer Science*, vol. 15, no. 2, p. 814, 2019.
- [43] N. Kathuria and B.-C. Seet, "24 GHz flexible antenna for Doppler radar-based Human Vital Signs Monitoring," *Sensors*, vol. 21, no. 11, p. 3737, 2021.
- [44] T. Yilmaz, R. Foster, and Y. Hao, "Detecting vital signs with wearable wireless sensors," (in eng), *Sensors*, vol. 10, no. 12, pp. 10837-10862, 2010, doi: 10.3390/s101210837.
- [45] Foster, Kenneth R., and Herman P. Schwan. "Dielectric properties of tissues." *CRC handbook of biological effects of electromagnetic fields* (1986): 27-96.
- [46] Augustine, Robin. "Electromagnetic modelling of human tissues and its application on the interaction between antenna and human body in the BAN context." PhD diss., Paris Est, 2009.
- [47] Vallejo, Mónica, Joaquín Recas, Pablo García Del Valle, and José L. Ayala. "Accurate human tissue characterization for energy-efficient wireless on-body

- communications." *Sensors* 13, no. 6 (2013): 7546-7569.
- [48] Iwamoto, Yumiko, Tatsuya Maruhashi, Yuichi Fujii, Naomi Idei, Noritaka Fujimura, Shinsuke Mikami, Masato Kajikawa et al. "Intima-media thickness of brachial artery, vascular function, and cardiovascular risk factors." *Arteriosclerosis, thrombosis, and vascular biology* 32, no. 9 (2012): 2295-2303.
- [49] Chami, Hassan A., Michelle J. Keyes, Joseph A. Vita, Gary F. Mitchell, Martin G. Larson, Shuxia Fan, Ramachandran S. Vasan, George T. O'Connor, Emelia J. Benjamin, and Daniel J. Gottlieb. "Brachial artery diameter, blood flow and flow-mediated dilation in sleep-disordered breathing." *Vascular medicine* 14, no. 4 (2009): 351-360.
- [50] Polak, Joseph F., Pamela Ouyang, and Dhananjay Vaidya. "Total brachial artery reactivity and first-time incident coronary heart disease events in a longitudinal cohort study: The multi-ethnic study of atherosclerosis." *PloS one* 14, no. 4 (2019): e0211726.
- [51] Safar, M. E., P. A. Peronneau, J. A. Levenson, J. A. Toto-Moukouo, and A. Ch Simon. "Pulsed Doppler: diameter, blood flow velocity and volumic flow of the brachial artery in sustained essential hypertension." *Circulation* 63, no. 2 (1981): 393-400.
- [52] F. Fantini, G. Barletta, R. D. Bene, C. Lazzeri, G. La Villa, and F. Franchi, "Parallel increase in carotid, brachial and left ventricular cross-sectional areas in arterial hypertension," *Journal of Human Hypertension*, vol. 11, no. 8, pp. 515–521, 1997.

- [53] Trazzi, Silvia & Santucci, Cinzia & Parati, Gianfranco & Mancia, Giuseppe. (1992). Variability in arterial diameter and compliance: compliance modulation reserve. *Journal of Hypertension*. 10.
- [54] Bank, Alan J., Daniel R. Kaiser, Scott Rajala, and Anthony Cheng. "In vivo human brachial artery elastic mechanics: effects of smooth muscle relaxation." *Circulation* 100, no. 1 (1999): 41-47.
- [55] Van Bortel, Luc M., Stephane Laurent, Pierre Boutouyrie, Phil Chowienzyk, J. K. Cruickshank, Tine De Backer, Jan Filipovsky et al. "Expert consensus document on the measurement of aortic stiffness in daily practice using carotid-femoral pulse wave velocity." *Journal of hypertension* 30, no. 3 (2012): 445-448.
- [56] Mihai, L. Angela, LiKang Chin, Paul A. Janmey, and Alain Goriely. "A comparison of hyperelastic constitutive models applicable to brain and fat tissues." *Journal of The Royal Society Interface* 12, no. 110 (2015): 20150486.
- [57] van Popele, Nicole M., Willem Jan W. Bos, Nicole AM de Beer, Deirdre AM van der Kuip, A. Hofman, Diederick E. Grobbee, and Jacqueline CM Witteman. "Arterial stiffness as underlying mechanism of disagreement between an oscillometric blood pressure monitor and a sphygmomanometer." *Hypertension* 36, no. 4 (2000): 484-488.
- [58] Brands, Peter J., A. P. G. Hoeks, M. C. M. Rutten, and R. S. Reneman. "A noninvasive method to estimate arterial impedance by means of assessment of local diameter change and the local center-line blood flow velocity using ultrasound." *Ultrasound in medicine & biology* 22, no. 7 (1996): 895-905.
- [59] Ecobici, Monica, And Claudiu Stoicescu. "Arterial Stiffness And Hypertension—Which Comes First?" *Maedica* 12, No. 3 (2017): 184.

